Theses and Dissertations   1. Thesis and Dissertation Collection, all items

2004-09

A novel approach to modeling the effects of radiation in Gallium-Arsenide solar cells using Silvaco's atlas software

Crespin, Aaron L.

Monterey, California. Naval Postgraduate School

http://hdl.handle.net/10945/1447

NAVAL POSTGRADUATE SCHOOL

MONTEREY, CALIFORNIA

THESIS

A NOVEL APPROACH TO MODELING THE EFFECTS OF RADIATION IN GALLIUM-ARSENIDE SOLAR CELLS USING SILVACO'S ATLAS SOFTWARE

by

Aaron L. Crespin

September 2004

Thesis Advisor:	Sherif Michael
Second Reader:	Gamani Karunasiri

Approved for public release; distribution is unlimited

THIS PAGE INTENTIONALLY LEFT BLANK

REPORT DOCUMENTATION PAGE			*Form Approved OMB No. 0704-0188*
Public reporting burden for this collection of information is estimated to average 1 hour per response, including the time for reviewing instruction, searching existing data sources, gathering and maintaining the data needed, and completing and reviewing the collection of information. Send comments regarding this burden estimate or any other aspect of this collection of information, including suggestions for reducing this burden, to Washington headquarters Services, Directorate for Information Operations and Reports, 1215 Jefferson Davis Highway, Suite 1204, Arlington, VA 22202-4302, and to the Office of Management and Budget, Paperwork Reduction Project (0704-0188) Washington DC 20503.			
1. AGENCY USE ONLY *(Leave blank)*	**2. REPORT DATE** September 2004	**3. REPORT TYPE AND DATES COVERED** Master's Thesis	
4. TITLE AND SUBTITLE: A Novel approach to Modeling the Effects of Radiation in Gallium-Arsenide Solar Cells Using Silvaco's ATLAS software			**5. FUNDING NUMBERS**
6. AUTHOR(S) Aaron L. Crespin			
7. PERFORMING ORGANIZATION NAME(S) AND ADDRESS(ES) Naval Postgraduate School Monterey, CA 93943-5000			**8. PERFORMING ORGANIZATION REPORT NUMBER**
9. SPONSORING /MONITORING AGENCY NAME(S) AND ADDRESS(ES) N/A			**10. SPONSORING/MONITORING AGENCY REPORT NUMBER**
11. SUPPLEMENTARY NOTES The views expressed in this thesis are those of the author and do not reflect the official policy or position of the Department of Defense or the U.S. Government.			
12a. DISTRIBUTION / AVAILABILITY STATEMENT Approved for public release; distribution is unlimited			**12b. DISTRIBUTION CODE**
13. ABSTRACT (maximum 200 words) The effects of radiation in GaAs solar cells has been extensively researched and the results of numerous investigation have yielded a considerable amount of information about the degradation in irradiated solar cells. This thesis establishes a novel method in which to use Silvaco's physically-based device simulator, ATLAS, to model the effects of radiation on solar cell output characteristics. A virtual model representing a single junction GaAs solar cell was created in ATLAS. The effects of radiation were modeled using carrier trapping statements representing the defects associated with various fluence levels of 1 MeV electron radiation which were characterized with Deep Level Transient Spectroscopy techniques. The resulting output characteristics of the virtual solar cell, illuminated with a simulated AM0 spectrum, were compared to published experimental measurements for GaAs solar cells of the same dimensions. The virtual solar cell demonstrated a good correlation between the measured and virtual solar cell output characteristics and accurate representation of the spectral response. Complete ATLAS and MATLAB codes are included in appendices.			
14. SUBJECT TERMS Solar cell, GaAs solar cell, radiation, electron, displacement damage, trap, ATLAS, Silvaco, GaAs, AlGaAs, physically based device simulation, simulation, model			**15. NUMBER OF PAGES** 85
			16. PRICE CODE
17. SECURITY CLASSIFICATION OF REPORT Unclassified	**18. SECURITY CLASSIFICATION OF THIS PAGE** Unclassified	**19. SECURITY CLASSIFICATION OF ABSTRACT** Unclassified	**20. LIMITATION OF ABSTRACT** UL

THIS PAGE INTENTIONALLY LEFT BLANK

A NOVEL APPROACH TO MODELING THE EFFECTS OF RADIATION IN GALLIUM-ARSENIDE SOLAR CELLS USING SILVACO'S ATLAS SOFTWARE

Aaron L. Crespin
Major, United States Marine Corps
B.S., United States Naval Academy, 1993

Submitted in partial fulfillment of the
requirements for the degree of

MASTER OF SCIENCE IN ELECTRICAL ENGINEERING

from the

**NAVAL POSTGRADUATE SCHOOL
September 2004**

Author: Aaron L. Crespin

Approved by: Sherif Michael
                     Thesis Advisor

                     Gamani Karunasiri
                     Second Reader

                     John P. Powers
                     Chairman, Department of Electrical and Computer Engineering

THIS PAGE INTENTIONALLY LEFT BLANK

ABSTRACT

The effects of radiation in GaAs solar cells has been extensively researched and the results of numerous investigation have yielded a considerable amount of information about the degradation in irradiated solar cells. This thesis establishes a novel method in which to use Silvaco's physically-based device simulator, ATLAS, to model the effects of radiation on solar cell output characteristics. A virtual model representing a single junction GaAs solar cell was created in ATLAS. The effects of radiation were modeled using carrier trapping statements representing the defects associated with various fluence levels of 1 MeV electron radiation which were characterized with Deep Level Transient Spectroscopy techniques. The resulting output characteristics of the virtual solar cell, illuminated with a simulated AM0 spectrum, were compared to published experimental measurements for GaAs solar cells of the same dimensions. The virtual solar cell demonstrated a good correlation between the measured and virtual solar cell output characteristics and accurate representation of the spectral response. Complete ATLAS and MATLAB codes are included in appendices.

THIS PAGE INTENTIONALLY LEFT BLANK

TABLE OF CONTENTS

LIST OF FIGURES

x

LIST OF TABLES

THIS PAGE INTENTIONALLY LEFT BLANK

ACKNOWLEDGMENTS

THIS PAGE INTENTIONALLY LEFT BLANK

EXECUTIVE SUMMARY

The military relies on satellite technology to fulfill communications and in informational requirements. In current satellite configurations, the use of solar cells is vital to power production. The exposure of these solar cells to the degrading effects of radiation is of great concern in ensuring power requirements are fulfilled throughout the expected life of a satellite. There are a variety of methods currently utilized to predict the effects of radiation on solar cell output characteristics. Current methods of prediction concentrate on determining a relationship between the output characteristics observed over various radiation fluence levels for a given type of radiation. These methods require exhaustive testing over a variety of material parameters to determine the constants within the mathematical estimations for output characteristics. Thorough testing to establish mathematical relationships for materials such as Silicon and Gallium-Arsenide has been accomplished; however, in the evolution of solar cell design, new materials and solar cell configurations are continuing to be developed. The endeavor to mathematically model the output characteristics as a function of radiation type and fluence will continue to be an expensive effort due to the extensive fabrication and testing required.

Previous theses by Andrew Bates and Max Green have established the ability of Silvaco's device simulator, ATLAS, to model solar cell configurations including multi-junctions solar cells. This thesis is an extension of these works, as it determines a novel method to accurately predict the effects of radiation utilizing this physically-based device simulator. This method differs from the current methods of prediction due to the methods of calculation employed by ATLAS. ATLAS uses a set of differential equations based on Maxwell's Laws to simulate the transport of carriers through a specified structure. In order to develop a model to predict the effects of radiation, it was necessary to concentrate on the relationship between the ATLAS modeling parameters and the physical results of radiation's interaction with semiconductor materials. The permanent degradation of solar cells which have been exposed to radiation is the result of damage to the crystal structure of the semiconductor material. This damage can be measured in terms of traps, which are energy levels created within the bandgap of the semiconductor mate-

rial. Through the use of Deep Level Transient Spectroscopy techniques, the characterization of traps induced by 1 MeV electron radiation in GaAs solar cell was investigated and published by Weng-Lyang Wang as part of his PhD dissertation at the University of Florida in 1984. This trap information, along with additional trap parameters, published in 1991 by Sheng S. Li and Robert Y. Loo in an article for *Solar Cells*, was used to model the effects of 1 MeV electron radiation in GaAs solar cells over various fluence levels. The virtual solar cell parameters were obtained from an article published in *IEEE Transactions on Electronic Devices*, written by Robert Y. Loo, Sanjiv Kamath, and Sheng S. Li in 1990.

ATLAS solar cell models were produced for four fluence levels of 1 MeV electron radiation. The result of simulation demonstrated an accurate representation of the solar cell measurements published in 1990. There was, on average, less than 3% difference between simulated and measured characteristics. The modeling of the virtual solar cell produced an accurate representation of the measured solar cell's spectral response.

I. INTRODUCTION

The military's use of satellites greatly enhances it's ability to communicate and gather information relative to the war fighter. Solar cells are today's primary source of power for satellite and space-based systems. These space-based systems rely on solar cells to meet overall system power requirements throughout their mission lives. Once in orbit, it is generally seen as prohibitively expensive, if not impossible, to repair or replace systems aboard spacecraft. Therefore, a considerable amount of research and planning are accomplished prior to launching systems bound for space. These systems are expected to endure harsh launch and operating environments and ultimately accomplish their mission requirements [Ref. 1].

One of the primary environmental concerns affecting solar cells in space is exposure to radiation. The space radiation environment consists of cosmic rays, electromagnetic radiation, Van Allen belt radiation, auroral particles, and solar flare particles [Ref. 2]. Exposure to radiation over extended periods of time has been shown to degrade the power generation capability of solar cells [Ref. 2]. This reduction in supplied electronic power can adversely affect satellite missions, especially if the end-of-life power available does not meet mission power requirements, resulting in partial or complete mission failures. As the costs of space missions are very high, considerable effort has been and continues to be expended to minimize the effects of radiation.

Current methods used to predict the effects of radiation in solar cells revolve around the development of mathematical expressions that reflect the measured outputs in reference to radiation fluence levels [Ref. 3]. This process requires extensive testing to determine the relationship of the output to the fluence levels for a single energy level of radiation. This process is further complicated by the multitude of parameters that can be varied within a solar cell design.

Green [Ref. 4] and Bates [Ref. 5] have experimented with modeling and optimizing multi-junction solar cell designs using the ATLAS device simulation software by Silvaco International [Ref. 6]. Their work demonstrated the usefulness of ATLAS as

a design tool for solar cells. As an extension of these works, this thesis incorporates a novel approach to modeling and predicting the effects of radiation in solar cells designed in ATLAS.

Chapter II provides a brief background discussion in semiconductor physics, solar cell operations and the nature of defects affecting solar cells. Chapter III describes the experimental measurements and values obtained from reference documentation. Chapter IV describes the software and modeling process utilized in simulating the referenced solar cells. Chapter V provides a comparison and discussion of the simulated and measured solar cell characteristics. Chapter VI notes the conclusions of this thesis and recommendations for future work in this area. Appendix A and B provide the ATLAS and MATLAB codes used to simulate the solar cells and radiation effects.

II.   BACKGROUND

This thesis presents a novel method to model the effects of radiation on solar cells. This chapter provides a brief discussion in basic semiconductor physics, solar cell operation and manufacturing processes. In addition, it also provides a brief description of radiation sources in space, their effect on solar cells, and the characterization of defects in semiconductors.

A.   SOLAR CELL BASICS

1.   Semiconductor Physics

There are several factors that govern the properties of semiconductors used in solar cells. Many of these properties are inherent to the atomic structure of the semiconductor material. Silicon (Si) is one of the predominant semiconductors currently in use and will be used to elaborate the basic concepts of semiconductor physics. Si is a Group IV element which alludes to the four valence electrons of an isolated Si atom has in its outer shell [Ref. 7]. When in the vicinity of other Si atoms these valence electrons are shared to form covalent bonds between atoms in order to fill the atoms outer shells as shown in Fig. 1a. These bonds allow for the formation of orderly crystal structures.
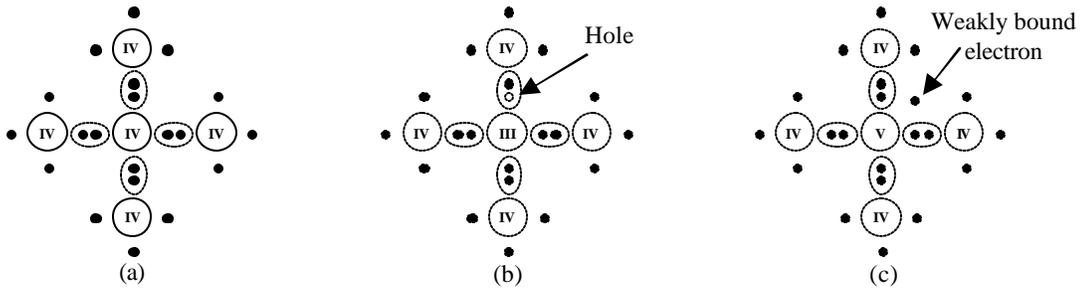
Figure 1.   Covalent bonds produced with (a) Group IV atoms, (b) Group III atoms, and Group V atoms [After Ref. 5.].

At a temperature of zero Kelvin, all valence electrons are contained in the valence band [Ref. 7]. When energy is imparted to these electrons, such as an increase in temperature, some of the electrons will break free from their parent atom and are free to move within the material. Free electrons will occupy the conduction band and the absence of these electrons results in the formation of a hole in the valence band, represented by an empty circle in Fig. 1. In a pure, flawless material, there are no stable energy states

between the conduction and valence bands, this forbidden region is called the band gap. The energy required for an electron to transition from the valence band to the conduction band is referred to as the bandgap energy, E_g [Ref. 7].

Conduction Band ● ● E_C

E_g

- - - - - - - - - - - - - - -

E_V
Valence Band ● ○ ● ● ○
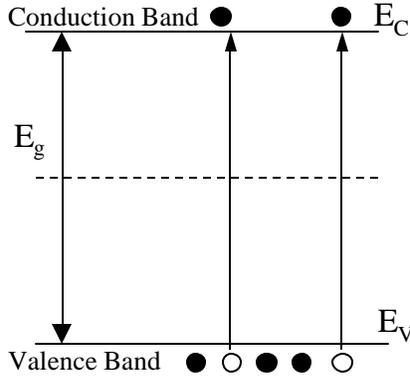
Figure 2.   Band gap diagram of a semiconductor [After Ref. 7.].

Controlling the number of electrons available for conduction is achieved through the addition of foreign atoms referred to as dopants. The selection of dopant atoms will determine if electrons are added or removed from the pool of electrons available for conduction. Group III and Group V elements can be used to dope Group IV materials [Ref. 5]. Atoms from Group III materials have three electrons in their outer shell and will form bonds with adjacent Si atoms. This will result in the formation of a hole as only seven of the eight available states in Si outer shell will be occupied as illustrated in Fig. 1b. Atoms from Group V materials have an extra electron which will be readily available for conduction as depicted in Fig. 1c. Negatively doped Si, n-type, is the result of doping with Group V atoms while positively doped Si, p-type, is the result of doping with Group III atoms. It is also possible to produce materials with semiconductor properties by combining Group III and Group V elements such as InP or GaAs. Addtionally, alloys of different mole fractions of Group III or Group V elements can be used to create ternary (three element) and quaternary (four element) semiconductors [Ref. 5].

A p-n junction is established when a p-type semiconductor is adjacent to an n-type semiconductor. The electrons in the n-type material will cross the junction to occupy available positions in the p-type material and fill the atom's outer shells as illustrated in Fig. 3a. This transition of electrons across the junction will result in a positive region within the n-type and a negative region within the p-type material known as the

4

space charge region [Ref. 7].   The positive and negative nature of the space charge region will create an electric field across the p-n junction [Ref. 7]. As this electric field increases, it will oppose the diffusion of electrons across the junction, stabilizing to the built-in potential, E_O, shown in Fig. 3b.
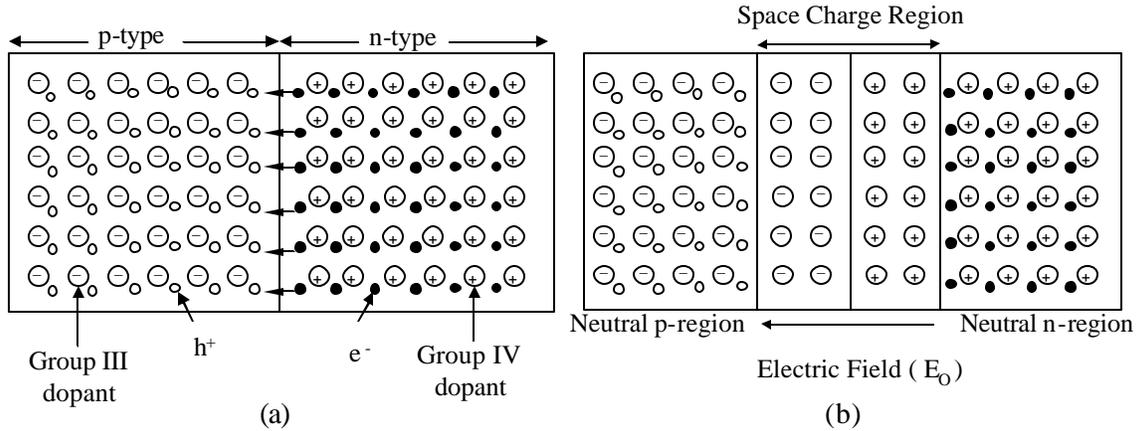
Figure 3.   p-n junction depicting (a) the diffusion of electrons, and (b) the space charge region and built-in electric field [After Ref. 7.].

2.   Solar Cell Operation

The formation of the space charge region in a p-n junction and the associated electrical field are vital to the operation of solar cells. A solar cell in its simplest form is a p-n junction with contacts on both ends to extract current. As light enters the solar cell, photons will impart energy to the electrons within the space charge region [Ref. 9]. Those photons with energies greater than E_g will free an electron and create a hole, known as an electron-hole pair (EHP). EHP's created in the space charge region will be immediately separated by the electric field within the region. The hole will drift towards the negative end of the electric field while the electron will drift towards the positive end as shown in Fig. 4 (1). When the electron reaches the neutral n-type region it will make this region negative. Likewise, the hole will make the neutral p-type region positive [Ref. 7]. An open circuit voltage is then created between the positive p-side and the negative n-side. EHP's created by photons outside the space charge region of the solar cell will diffuse based on carrier concentrations as there is no electric field with which to interact. The minority carrier of an EHP created within close proximity to the space charge region can travel the distance to the space charge region and be swept by the electric field adding to the potential charge in the solar cell as shown in Fig. 4 (2 and 2').

5

This distance, called the minority carrier diffusion length, is the mean distance an electron, L_e, or hole, L_h, can travel before recombining with an opposite charge [Ref. 7]. If an EHP is created outside the minority carrier diffusion length, the minority carrier will recombine with an opposite charge and will not add to the accumulation of potential charge in the cell, Fig. 4 (3 and 3').

Anode

Neutral p-region

2'   3'

E_O 1

2

3

Neutral n-region

Cathode
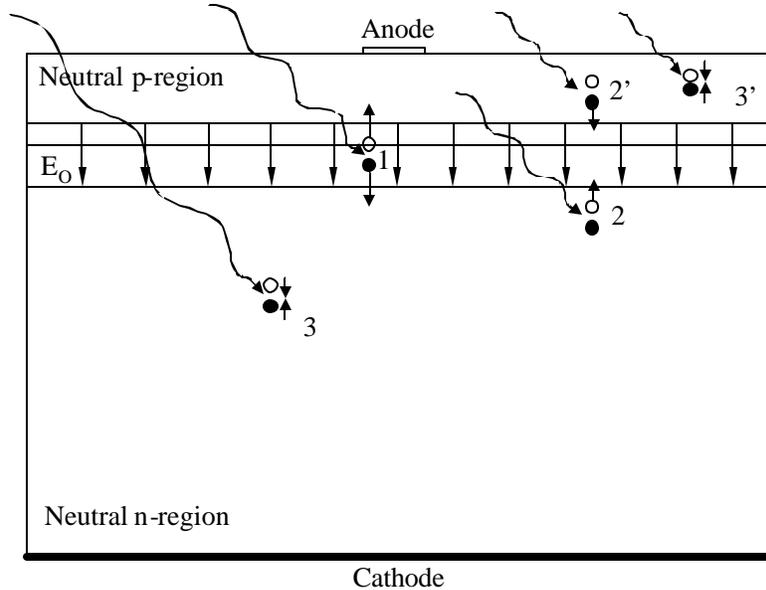
Figure 4.   Electron-hole pair generation within the space charge region (1) ,minority carrier diffusion length (2 and 2'), and neutral regions of a solar cell(3 and 3').

Solar cell output characteristics can vary depending on cell configurations, types of material used, doping levels, and region thicknesses. In order to compare various cells, several standard parameters have been established. Many of these parameters can be expressed graphically on a current-voltage characteristics curve or *I-V* curve (see Fig. 5). The limits of solar cell operations are set by the open circuit voltage, V_{OC}, and the short circuit current, I_{SC} [Ref. 9]. The V_{OC} is potential created by the accumulation of charge swept to either end of the space charge region while the solar cell is illuminated in an open circuit condition. The short circuit current is the measure of current expected in shorted condition. On the *I-V* curve, V_{OC} is voltage corresponding to zero current and I_{SC} is the current corresponding to zero voltage [Ref. 9]. The product of current and voltage pairs along the *I-V* curve correspond to an output power and the maximum output power, P_{max}, is generally located near the knee in the *I-V* curve [Ref. 9].
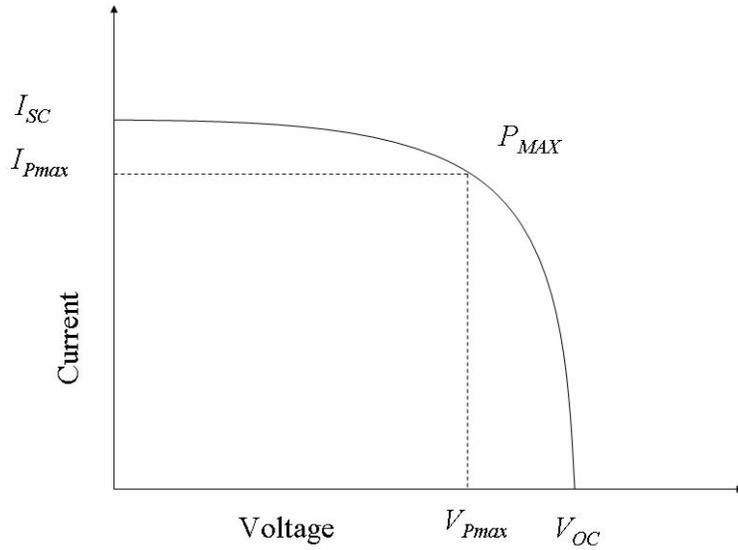
Figure 5.   Typical *I-V* curve of a solar cell.

Two other measurements by which solar cells are compared are fill factor, FF, and efficiency, ?. The FF is the ratio of P_{max} to the product of I_{SC} and V_{OC} [Ref. 9]. Graphically, the FF is a measure of the sharpness of the knee in the solar cells *I-V* curve. The efficiency of a solar cell is the ratio of P_{max} to the incident light power on the solar cell, P_{avail} [Ref. 9]. The equations are [Ref. 9]

$$FF = \frac{P_{\max}}{I_{SC}V_{OC}}$$ (0.1)

$$h = \frac{P_{\max}}{P_{avail}}.$$ (0.2)

Another quantity that can be used to compare solar cells is the spectral response. The spectral response is the number of electrons generated at a given wavelength relative to the number of photons incident upon the solar cell at that wavelength, also known as quantum efficiency (QE) [Ref. 9]. The internal spectral response is defined as the number of EHP's collected under short circuit conditions, I_{SC}, compared to the number of photons entering the cell [Ref. 9]. The external spectral response is the internal spectral response taking into account the reflection of light at the surface [Ref. 9]. Spectral re-

7

sponse can be regarded as a measure of how efficiently a solar cell converts a given wavelength of light to usable current.

3. Growth Methods and Grown-in Defects

In a search to produce higher efficiency solar cells, various methods of material growth have been developed. Each successive process has increased the purity and quality of the crystals produced. There are several methods for growing III-V compounds such as Gallium-Arsenide, GaAs. These can be separated into two basic categories: bulk growth and epitaxial growth. The two bulk growth methods include Liquid Encapsulated Czochralski (LEC) and the Bridgman method [Ref. 10]. The LEC grows a single crystal of GaAs from a molten liquid. The basic technique is modified due to Arsenic's volatility at Gallium's melting temperature. The liquid is covered with a layer of boron trioxide and a high pressure inert gas to prevent the evaporation of As. The Bridgman method uses a two-zone technique where a crucible is pulled from one side of a tube where the temperature is above the melting point of Ga to the other side where the temperature is reduced to accommodate As [Ref. 10].

Epitaxial growth methods are characterized by the growth of one crystal upon another [Ref. 10]. This growth can be of the same compound, known as homoepitaxy, or of a different compound from the substrate, heteroepitaxy. Various methods used in epitaxial growth include Liquid Phase Epitaxy (LPE), Chemical Vapor Decomposition (CVD), Molecular Organic Chemical Vapor Deposition (MOCVD), and Molecular Beam Epitaxy (MBE) [Ref. 10].

Liquid Phase Epitaxy (LPE) deposits layers of material while they are in the liquid phase. When impurities are added to the liquid material, the melting point is reduced. As the resulting solution is cooled, new layers form on the seed crystal. As the crystal grows, the concentration of impurities in the liquid begins to increase, allowing a further drop in temperature. The rate of crystal growth is controlled by the rate of temperature reduction [Ref. 10].

Chemical Vapor Deposition (CVD), also known as Vapor Phase Epitaxy (VPE), grows crystals from gaseous compounds containing Ga and As. These compounds react on the substrate to form GaAs and byproducts of the remaining elements [Ref. 10].

Metal Organic Chemical Vapor Deposition (MOCVD) is a specific type of CVD growth process. Metalorganic compounds are used to produce both the main elements and doping elements. This method is known to produce high quality material with large mobilities and minority carrier lifetimes [Ref. 10].

Molecular Beam Epitaxy (MBE) is a technique where gaseous beams of molecules interact with a crystal surface under ultra-high-pressure to form an epitaxial layer. The high standard of cleanliness and vacuum conditions, permit a very high level of purity in the materials grown [Ref. 10].

The quest for high quality material is an attempt to reduce the number of defects in crystal structures and their effects on carrier lifetimes. Defects can be categorized as point, linear, or planar [Ref. 7]. Point defects may consist of interstitial atoms, vacancies and substitutional impurities in the crystal, Fig. 6a. Linear defects include edge and screw dislocations, Fig. 6b, while planar defects occur at grain boundaries, Fig. 6c. These defects are disruptions in the crystal pattern that permit energy states within the bandgap. These states are occupied by carriers during operation and affect carrier lifetimes, diffusion lengths, and increase the probability of recombination. Another source of defects within the solar cell crystal structure is the result of events external to the solar cell such as radiation.

(a)   (b)   (c)
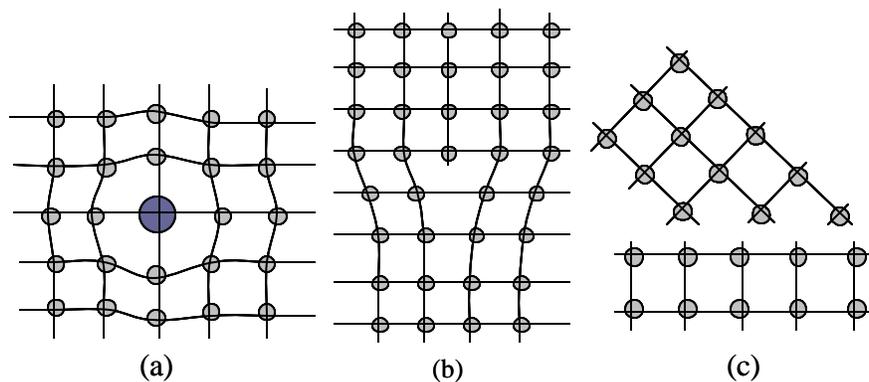
Figure 6.   Types of defects: (a) point, substitutional defect, (b) linear, dislocation defect, (c) planar, grain boundary defect [After Ref. 7.].

B. RADIATION

1. Sources of Radiation

Radiation of concern to solar cells in space can come from a variety of sources. These may include electrons and protons trapped in the geomagnetic field, radiation associated with solar flares, and galactic cosmic ray radiation to a small extent [Ref. 3]. This radiation can be classified as one of two types: electromagnetic or particulate radiation. Electromagnetic radiation consists of light, X-rays, and gamma rays; particulate radiation consists of electrons, protons, neutrons, alpha particles, and others with a finite rest mass [Ref. 3]. Particle radiation can be characterized by the energy level of the particle and fluence of the radiation encountered. The energy level is defined by units of electron volts (eV) which is equivalent to 1.6×10^{-19} joules. Fluence is defined by the total particles per area in a given time period with units of particles per cm^2.

2. Effects of Radiation on Solar Cells

Radiation can interact with solar cells in a variety of ways but the primary damage mechanisms of interest in solar cell degradation are ionization and displacement damage [Ref. 3]. Ionization occurs when bound electrons are removed from their parent atoms. Radiation can affect solar cell outputs through several ionization related effects. These include the reduction of coverglass transmittance, darkening of transparent polymers, and altering of polymers mechanical properties [Ref. 3]. Ionizing radiation can also produce EHP in the same manner as light does but the energy level required to create an EHP is significantly greater than associated with light [Ref. 3]. The other mechanism, displacement damage, occurs when radiation dissipates energy to the solar cell, resulting in the displacement of an atom from its position within the crystal structure. When an atom is displaced, a vacancy is created, along with an interstitial atom, also known as a Poole-Frenkel defect, Fig. 7 [Ref. 11]. Higher energy radiation can have the effect of displacing multiple atoms in an elastic collision cascade [Ref. 11]. Radiation-induced defects result in energy states within the band gap similar to those created by grown-in defects. These energy states result in trapping and recombination centers throughout the solar cell material [Ref. 11].
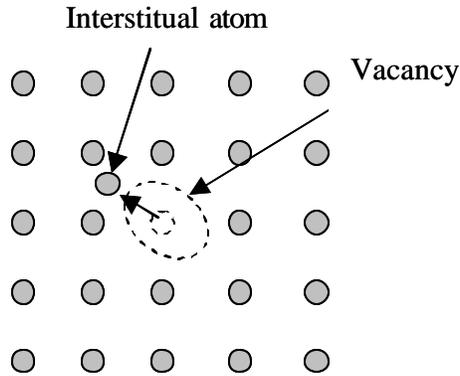
Figure 7.   Poole-Frenkel defect.

3.   Recombination and Capture of Electrons and Holes

Figure 8 shows a series of electron transitions that will be used to illustrate re-combination and carrier capture. Fig. 8a represents the transitions associated with the absorption of light in the fundamental band and localized traps [Ref. 11]. Transition 1 represents the generation of an electron hole pair as an electron is excited directly from the valence band. Transition 2 represents an electron excited from a bound state resulting in a free electron and a bound hole. Transition 3 is an electron excited from the valence band to a trap resulting in a free hole [Ref. 11]. Electrons and holes produced as a result of photo-ionization will exist until captured by a trap. Traps can exist as either trapping centers or recombination centers [Ref. 11]. Trapping centers exist at energy levels closer to the conduction or valance band. Carriers captured by trapping centers have a higher probability of being thermally excited back to a free state [Ref. 11]. Recombination centers exist at energy levels closer to the center of the band gap and carriers captured have a higher probability of recombination with a carrier of the opposite charge [Ref. 11].
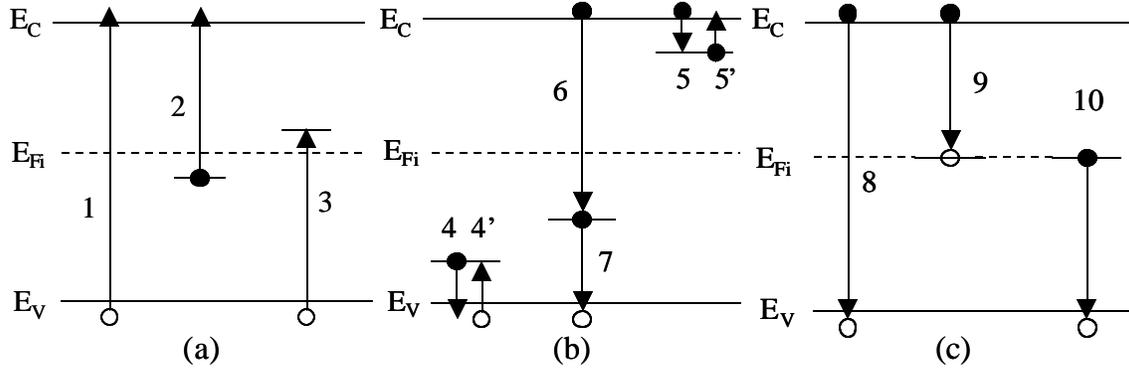
Figure 8.   Electron transitions: (a) photoionization, (b) carrier capture, and (c) recombination [From Ref. 11.].

In Fig. 8b, the processes 4, 4', 5, and 5' represent the capture and thermal excitation of carriers in trapping centers [Ref. 11]. The transition 6 in Fig. 8b represents the capture of an electron by a recombination center and transition 7 is the capture of a hole. Temperature plays a significant role in whether a trap will act as a trapping or recombination center. Figure 8c represents transitions associated with recombination. The transition 8 is the direct recombination of a free electron and a free hole. The release of a photon is associated with this type of recombination but the probability of this event is low [Ref. 11]. The transitions 9 and 10 represent the more likely cases of capturing an electron and hole, respectively [Ref. 11]. Excess energy from this transition can be dissipated through photons, phonons, or the Auger effect. The Auger effect occurs when the energy of two recombining carriers is transferred to a third carrier resulting in impact recombination [Ref. 11].

C.   CHARACTERIZATION OF TRAPS

Traps can be characterized by various parameters to include the type of carrier they can be expected to capture, energy level, capture cross section, and the density of a specific trap encountered.

1.   Trap Type and Energy Level

Traps are defined as electron or hole traps depending on which carrier they can expect to capture. Electron traps are expected to trap electrons from the conduction band and the trap energy level, E_t, is measured from the conduction band to the local trap en-

12

ergy level. Hole traps are expected to capture holes from the valence band and their energy level is measure from the valence band to the local trap level, Fig. 9 [Ref. 11].
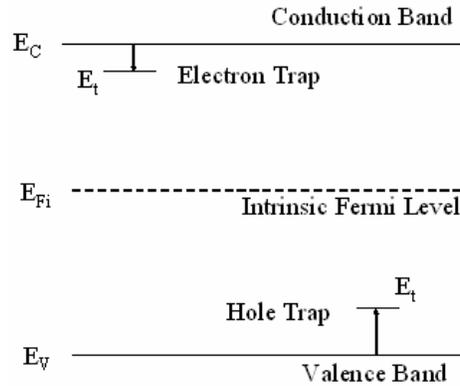
Figure 9.   Carrier traps and energy levels.

2.   Capture Cross Section

Carrier lifetime is not generally governed by direct recombination, but by the presence of defects [Ref. 11]. Recombination at traps is influenced by the occupation of these traps by carriers. The extent of occupation is related to the carrier density through the probability of capture by a vacant trap known as the capture cross section, s [Ref. 11]. The value of the capture cross section is determined by the potential near the trap. Traps whose electric charge attracts a carrier of opposite charge have large capture cross sections, Fig. 10a. Neutral traps for a single displaced atom would have a capture cross section on the order of the atomic cross section of the displaced atom, Fig. 10b [Ref. 11]. Centers whose charge is the same as a carrier will be surrounded by a potential barrier causing electrostatic repulsion, resulting in a very low capture cross section as seen in Fig. 10c. A single displaced Arsenic atom within the crystal structure will be used to illustrate the nature of the capture cross section. Assuming the displaced atom creates a negative trap when displaced, the displaced atom will have a large potential for capturing holes. Once the trap has been occupied by a hole through the emission of an electron, it becomes neutral in charge and now has a smaller capture cross section for capturing electrons.

13
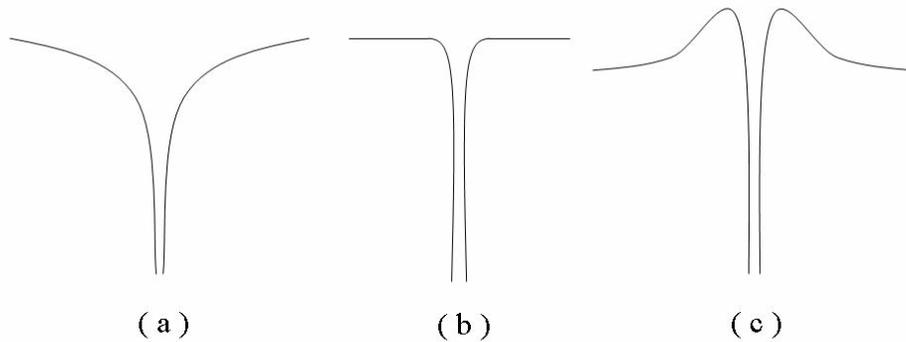
Figure 10.   Representation of capture cross sections; (a) opposite, (b) neutral, and (c) like charges with an attractive center [From Ref. 11.].

3.   Trap Density

The number of traps in a given volume is defined as the trap density, N_t. There exists a linear relationship between trap densities and radiation fluence. As the fluence level increases, the density of traps also increases by a constant factor that is the product of atoms per unit volume, n_a, capture cross section, s, and average displacements per primary displacement, ? [Ref. 3], given by

$$N_t = n_a \boldsymbol{s} \boldsymbol{n} \Phi .$$
(0.3)

As the number of particles irradiating the material increases, the quantity or density of traps increases, but the type of damage created remains constant for a specific type of radiation at a given energy level.

D.   SUMMARY

The background information introduced in this chapter is intended to provide the reader with the basic concepts and definitions to be used in the following chapters. The relationships and definitions provided are the basis for the development of a technique to predict the effects of radiation on a solar cell using ATLAS. This information also clarifies the discussion of techniques and information annotated in the referenced experiments.

III.   EXPERIMENTAL SOLAR CELL

This chapter describes the physical structure and the measured the output characteristics of the referenced solar cells. It also presents the defects resulting from electron radiation and describes the experimental methods used to in characterizing these defects.

A.   SOLAR CELL REFERENCES AND PARAMETERS

The experimental data for this thesis comes from three published sources [Ref. 12, 13, and 14]. The solar cells used for the experimental and structural data were described in Ref. 12, which is a study in radiation damage and annealing in GaAs solar cell's.   Reference 12 provided information pertaining to the irradiation of the solar cells at room temperature with 1 MeV electrons at fluences ranging from $1x10^{14}$ to $1x10^{16}$ electrons/cm^2. The defect parameters were published in Ref. 13, which provided an overview of native and radiation induced defects in GaAs. Reference 13 is based in part on Ref. 14, which is a study in grown-in and radiation induced defects and is the source of the experimental methods for defect characterization.

1.   Structural Parameters

The solar cell from Ref. 12 was built as a p-on-n GaAs cell using the LPE growth method. The solar cell structure as shown in Fig. 11 consisted of three layers on an n$^+$-GaAs substrate with a doping concentration of $5x10^{17}$ cm^{-3}. The n-GaAs base was immediately above the substrate with a thickness of 10 μm and had doping concentration of $1x10^{17}$ cm^{-3}. Above the base was a p-type GaAs emitter with a thickness of 0.5 μm and a doping concentration of $1x10^{18}$ cm^{-3}. The window layer was made of AlGaAs and had a thickness of 0.5 μm. The molar fraction of the $Al_XGa_{1-X}As$ was listed as 0.95 and the doping concentration was $1x10^{18}$ cm^{-3}. The anode contact was made of AuZn with a thickness 300 nm and had a 4 μm layer of silver. The cathode contact was made of AuGeNi with silver overlay. The solar cell was produced with a Tantalum oxide, Ta_2O_5, antireflective coating but was not provided cover glass protection [Ref. 12].

Anode			
Window	Al$_{0.95}$Ga$_{0.05}$As	0.5 µm	N$_D$=1x10^{18}cm^{-3}
Emitter	p-GaAs	0.5 µm	N$_D$=1x10^{18}cm^{-3}
Base	n-GaAs	10 µm	N$_D$=1x10^{17}cm^{-3}
Substrate	n$^+$-GaAs		N$_D$=5x10^{17}cm^{-3}
Cathode			

Figure 11.   Referenced GaAs solar cell structure.

B.   METHODS OF MEASUREMENT

Many of the defects described in Ref. 13 were based on the work of Weng-Lyang Wang while at the University of Florida. Wang's PhD dissertation [Ref. 14] annotates several methods utilized to extract the damage parameters resulting from electron radiation. These included current-voltage characterization, thermally stimulated capacitance and deep level transient spectroscopy.

1.   Current-Voltage (I-V) Characterization

Measuring the current-voltage characteristics of a p-n junction diode, in the forward bias region, can reveal information concerning the recombination process within the space charge region [Ref. 14]. The total current in a p-n junction diode is a combination of the diffusion current and the generation-recombination current in the space charge region. When the generation-recombination current dominates the current expression the effective carrier lifetimes can be derived from the magnitude of the generation-recombination current. The density of traps, N_t, and capture cross section, s$_n$, were calculated using the carrier lifetimes defined with reference to the average thermal velocity, ?$_{th}$, as

$$\boldsymbol{t}_n = \frac{1}{N_t \boldsymbol{s}_n \boldsymbol{n}_{th}}. \tag{3.1}$$

16

2. Thermally Stimulated Capacitance (TSCAP)

Another technique used to calculate trap densities is known as the thermally stimulated capacitance (TSCAP) measurement [Ref. 14]. TSCAP was accomplished by reverse biasing a p-n diode and then cooling the temperature to that of liquid nitrogen (77 K). The diode was briefly zero biased and then reversed biased [Ref. 14]. This allowed the majority carrier traps to be filled. The temperature was then raised to around 400 K. A thermal scan of the capacitance, C, verses temperature, T, was plotted. If carrier emission were taking place a capacitance step was observed on the C vs. T plot. The amplitude of the capacitance step is proportional to the trap density.

3. Deep Level Transient Spectroscopy (DLTS)

Deep Level Transient Spectroscopy (DLTS) was introduced by Lang in 1974 as a technique to study deep levels in semiconductors [Ref. 3]. Deep levels in the depletion region of a p-n junction can be filled with charge carriers by an electrical pulse [Ref. 14]. The capacitance transient is monitored as the temperature is increased at a constant rate and a DLTS spectrum is produced. This spectrum is used to extract trap parameters within the tested region. These characteristics include the trap energy, E_t, capture cross section, $s_{n,p}$, and trap density, N_t. An example of the DLTS spectrum is shown in Fig 12.
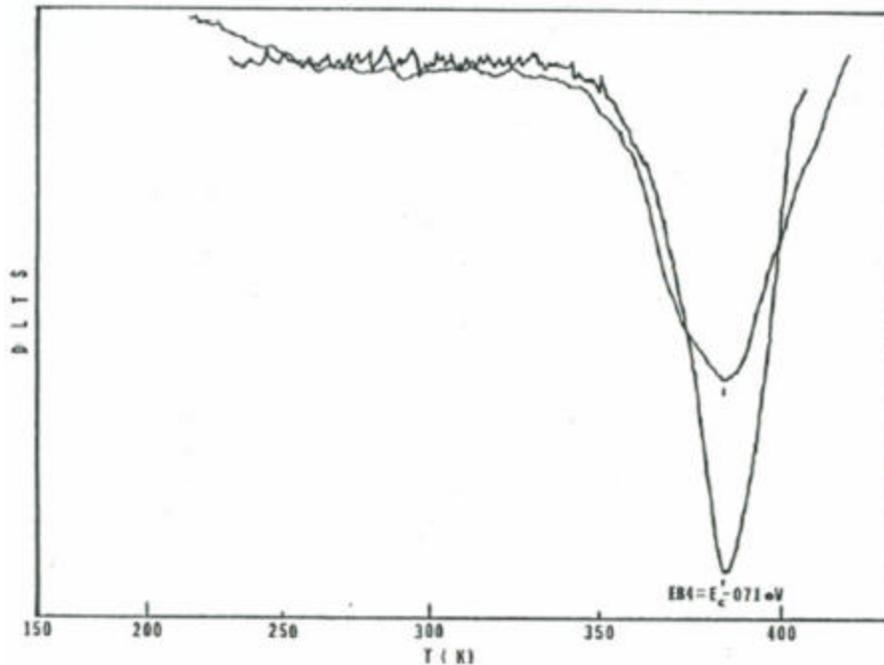
Figure 12.   DLTS scans of electron traps for two LPE GaAs samples [From Ref. 14].

C. EXPERIMENTAL MEASUREMENTS

1. Measured Trap Values

A thorough description of electron and hole trap information for both native and radiation induced defects was collected by S. S. Li and R. Y. Loo [Ref. 13]. Trap data was available for various fluence levels and temperatures. The values listed in Table 1 are traps measured in specimens irradiated at 25°C across three fluence levels of electron radiation [Ref. 12]. The range of data at this temperature provided enough detail to accurately characterize the effects of electron radiation over a wide range of fluences. Table 1 is partitioned into electron and hole traps with respect to electron fluence levels. Each trap is identified by energy level, density, and capture cross section for the specified carrier. Electron traps were measured in the n-GaAs region while the hole traps were measured in the p-GaAs regions of the mesa diodes. Data marked with an asterisk were not provided in the references and was subsequently estimated based on traps with similar energy levels or the linear relationships between fluence and density, as previously discussed.

Table 1.   Experimentally measured electron and hole traps in n- and p-GaAs [From Ref. 13].

Fluence F_e (cm^{-2})	Electron traps in n-GaAs			Hole traps in p-GaAs		
	E_t (eV)	N_t (cm^{-3})	s_n (cm^{-2})	E_t (eV)	N_t (cm^{-3})	s_p (cm^{-2})
10^{14}	E_C-0.14	1.8×10^{13}	5.7×10^{-13}	E_V+0.71	3.0×10^{12}	2.2×10^{-13}
	E_C-0.41	8.2×10^{12}	2.6×10^{-13}			
	E_C-0.71	$7.0 \times 10^{12*}$	8.3×10^{-13}			
	E_C-0.90	8.8×10^{11}	3.0×10^{-11}			
10^{15}	E_C-0.41	$3.0 \times 10^{13*}$	2.6×10^{-13}	E_V+0.13	2.2×10^{14}	$2.6 \times 10^{-13*}$
	E_C-0.71	1.7×10^{13}	8.3×10^{-13}	E_V+0.29	4.0×10^{14}	2.6×10^{-13}
	E_C-0.90	2.8×10^{13}	3.0×10^{-11}	E_V+0.35	8.0×10^{13}	7.2×10^{-15}
				E_V+0.71	6.4×10^{13}	2.2×10^{-13}
10^{16}	E_C-0.41	8.8×10^{13}	2.6×10^{-13}	E_V+0.13	8.4×10^{14}	$2.6 \times 10^{-13*}$
	E_C-0.71	5.0×10^{13}	8.3×10^{-13}	E_V+0.29	1.6×10^{15}	2.6×10^{-13}
	E_C-0.90	6.5×10^{14}	3.0×10^{-11}	E_V+0.35	1.0×10^{15}	7.2×10^{-15}
				E_V+0.71	2.7×10^{14}	2.2×10^{-13}
* interpreted values based on similar trap energy levels and linear relationships						

Figure 13 is provided to confirm the linear relationship of trap densities with fluence levels. The linear relationship holds for those traps with data available over three fluence levels. The exception to this would be the hole trap at an energy level of 0.71 eV above the conduction band at a fluence level of 10^{15} e/cm^2. This trap density appears to be higher than would be expected in relation to the trap measurements at the two adjacent fluence levels.
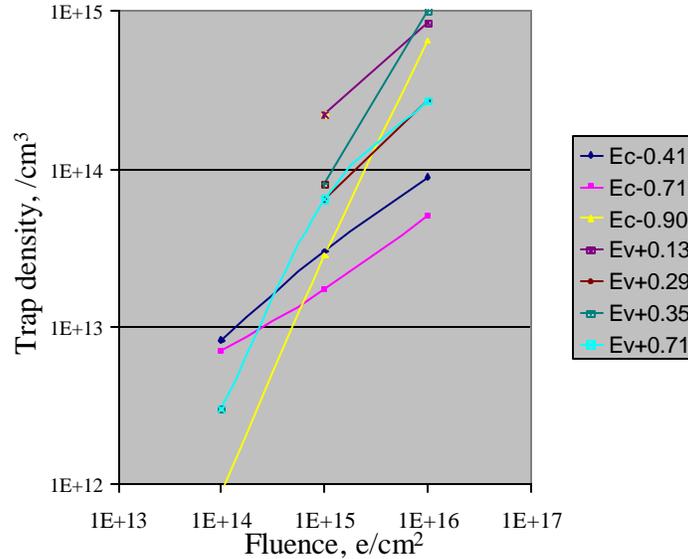
Figure 13.   Experimentally measured trap densities in relation to fluence levels [After data from Ref. 13.].

2.   **Measured Output Chracteristics**

The data available for solar cell output characteristics was normalized to the pre-radiation output values. Figure 14 is a plot of measured I_{SC}, V_{OC} and the fill factor for fluence levels up to 1×10^{16} e/cm^2. The output characteristics are shown to degrade with an increase in radiation fluence. The I_{SC} displays a 40% reduction in current from its pre-radiation value while V_{OC} displays approximately a 15% drop in voltage [Ref. 12]. The fill factor shows little degradation over the range of fluence values. Graphically, this would be seen as a decrease in the size of the *I-V* curve while the general shape of the curve remains constant.
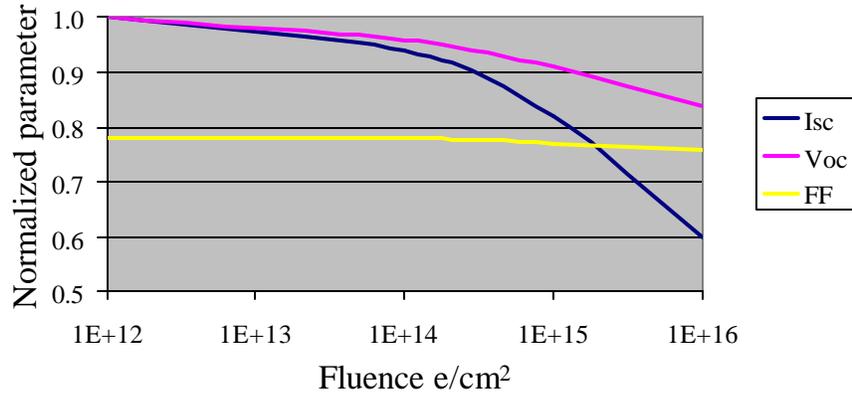
Figure 14.   Normalized short circuit current, open circuit voltage, and fill factor [After experimental data from Ref. 12.].

The maximum power and solar cell efficiency are shown in Fig. 15. The P_{max} prior to irradiation was 21.25 mW and drops to 53% of it original value at a fluence level of $1x10^{16}$ e/cm^2 [Ref. 12]. The solar cell efficiency has a pre-irradiation value of 15.7 % and deteriorates to 8.3 % efficiency at the highest level of fluence [Ref. 12].
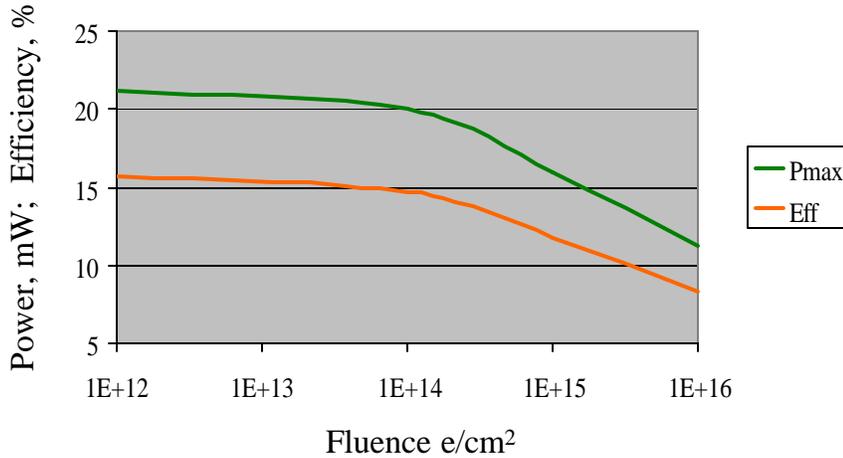
Figure 15.   Experimentally measured P_{max} and efficiency in relation to radiation fluence levels [after data from Ref. 12].

D.   SUMMARY

The output characteristics and trap parameters provided by the referenced documents provide a basis for comparison of ATLAS simulations in the following chapter. The bulk of the information gleaned from the references is in adequate detail to produce a comparable model in ALTAS. The experiments were specifically tailored to support the subjects of the referenced articles. A lack of detail is provided in the range of error for

20

measurements and number tested. A more thorough investigation into differences in simulated and measured values would be possible had the data been specifically tailored for the purpose of validating the ATLAS model. The following chapter provides a brief description of ATLAS and a detailed discussion of modeling an equivalent GaAs solar cell.

THIS PAGE INTENTIONALLY LEFT BLANK

IV. SOLAR CELL SIMULATION

This chapter presents the radiation modeling approach and discussion of parameter selection decisions. The measured solar cell parameters and output characteristics discussed in the previous chapter were the benchmarks for the simulations. The measured trap details provided the foundation for modeling radiation damage in the virtual solar cells.

A. THE SILVACO ATLAS DEVICE SIMULATOR

ATLAS is a physically based two- and three-dimensional semiconductor device simulator [Ref. 6]. Physically based device simulators predict the electrical behavior associated with the physical structure under specified biased conditions. ATLAS achieves this through partitioning the specified device into a two or three-dimensional mesh grid. ATLAS then applies a set of differential equations, based on Maxwell's Laws, to the mesh to simulate the transport of carriers through the structure [Ref. 6].

Interface with ATLAS is provided through Silvaco's Deckbuild run-time environment via an ASCII text file. Structure and command inputs to ATLAS are required to simulate a device [Ref. 6]. The structure data contains the dimensions, material characteristics, and mesh grid parameters of the device desired. The command file identifies the commands ATLAS will execute in order to provide the desired output. The order in which statements are specified to ATLAS is significant and must conform to the following precedence: structural specifications, material models specifications, numerical method selection, solution specification, and then results analysis [Ref. 6]. Additionally, the order within each of these specifications is also significant. For example, when identifying the structure specifications, the required command order is mesh, region, electrodes, and then doping. Failure to adhere to the specified order will result in ignored statements, incorrect simulation results and/or program termination. The ATLAS code for simulating the various models used for this thesis is provided in Appendix A.

B. THE VITUAL SOLAR CELL MODEL

The experimental solar cell's material and dimensions were modeled as specified in Chapter III with a few exceptions. Some parameters, not identified by the references, were estimated while other parameters could not successfully be modeled on the current

version of ATLAS. A separate solar cell model was created to represent each level of radiation. The damage as a result of radiation was represented through a series of trap statements within the material model specification portion of the code.

1. ATLAS Calculations

ATLAS uses a mathematical model that operates on any semiconductor device. This model consists of a set of fundamental equations which link together the electrostatic potential and carrier densities [Ref. 6]. The primary equations derived from Maxwell's laws consist of Poisson's Equation, the continuity equations and transport equations. Poisson's Equation relates variations in electrostatics potential to local charge densities

$$\text{div}(e \nabla y) = -r , \qquad (4.1)$$

where y is the electrostatic potential, e is the local permittivity, and r is the local space charge density. The electric field is obtained from the gradient of the potential

$$\bar{E} = \nabla y , \qquad (4.2)$$

where $\bar{E}$ is the electric field. The continuity and transport equations describe the way carrier densities are calculated as a result of transport, generation and recombination processes [Ref. 6]. The continuity equations for electrons and holes are

$$\frac{\partial n}{\partial t} = \frac{1}{q} \text{div} \overrightarrow{J_n} + G_n - R_n , \qquad (4.3)$$

$$\frac{\partial p}{\partial t} = \frac{1}{q} \text{div} \overrightarrow{J_p} + G_p - R_p , \qquad (4.4)$$

where n and p are the electron and hole concentrations, $\bar{J}_n$ and $\bar{J}_p$ are the current densities, G_n and G_p are the generation rates, R_n and R_p are the recombination rates, and q is the electron charge.

2. Virtual Solar Cell Parameters

The virtual solar cell shown in Fig. 16, was modeled, when possible, according to the dimension and material characteristics specified in Chapter III. The reference documentation does not identify the width of the anode contact or the thickness of the cells substrate. When creating the virtual solar cell structure, the anode contact width was

modeled to be 8% of the cell's surface area and the substrate thickness was modeled as 200 µm. Additionally, the virtual cell was designed to produce an output for a 1 cm^2 cell area, where the referenced cells had areas of 4 cm^2.
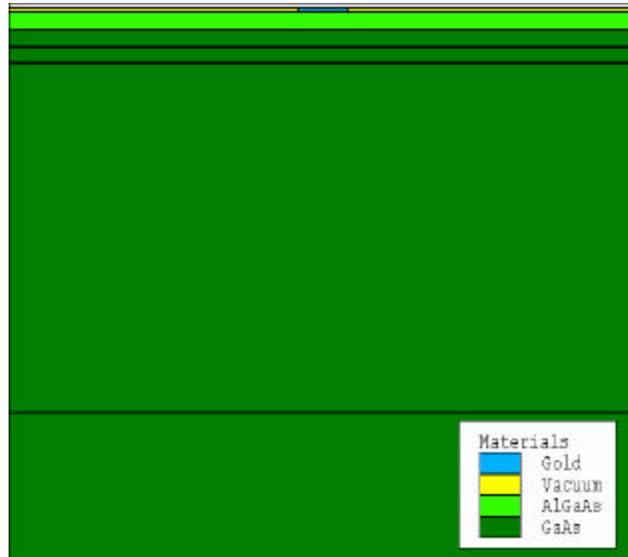
Figure 16.   Structure of the virtual solar cell produce in Tony Plot.

The referenced solar cells were illumination by an unspecified Air Mass Zero (AM0) spectrum simulator. The virtual solar cell was illuminated with the most current AM0 spectrum file, Fig. 17, identified by the Renewable Resource Data Center, National Renewable Energy Laboratory (NREL) [Ref. 15]. The virtual solar cell contacts were modeled as pure gold for optical characteristics only; no resistance was associated with the modeled contacts. External lump series resistance simulations were unsuccessful on the current version of ATLAS. A five percent reflection of incident light upon the first layer was used to model the typical effects of the solar cell's Ta$_2$O$_5$ antireflective coating [Ref. 5].
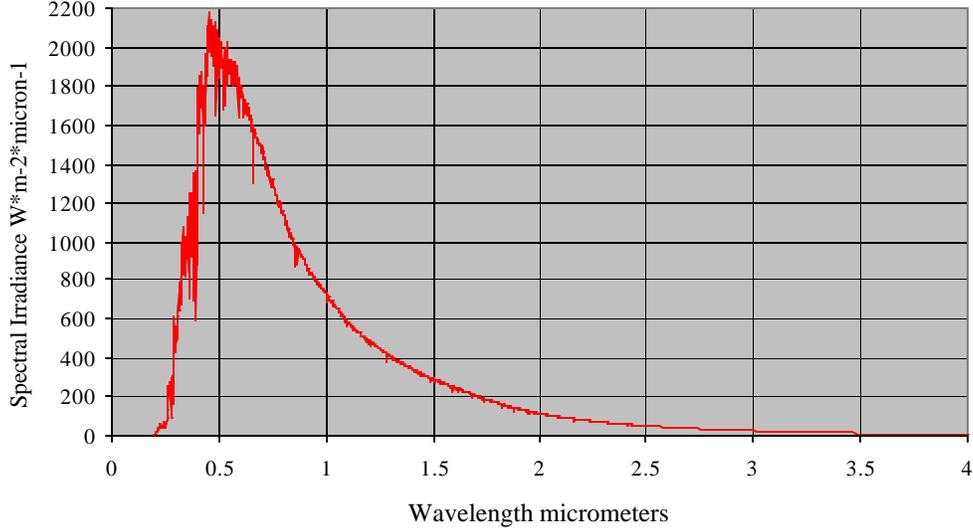
Figure 17.   Air Mass Zero spectrum file used in model illumination [From Ref. 15.].

Significant interaction occurs within the space charge region and the minority carrier diffusion length. To ensure adequate calculations over these regions, it was necessary to build a solar cell structure that specifically identified the space charge region. The static space charge region was identified in the model based on the calculated depletion region widths from [Ref. 7]

$$W = \left[\frac{2e(N_A + N_D)E_o}{qN_A N_D} \right]^{\frac{1}{2}},$$
(4.5)

where W is the depletion width, e is the local permittivity, N_A is the acceptor doping concentration, N_D is the donor doping concentration, E_o is the built in potential, and q is the charge of an electron [Ref. 7]. The complete depletion width is the total sum of the p- and n-region depletion region widths, shown by

$$W = W_n + W_p,$$
(4.6)

where W_n is the width of depletion region in the n-region and W_p is the width of the depletion region into the p-region. These widths were modeled to reflect the depletion

depths into the n- and p-regions from the charge on one side of the depletion layer given by

$$|Q| = qN_dW_nA = qN_aW_pA,$$ (4.7)

where A is the area of the junction [Ref. 7]. Manipulation of Eqns 4.6 and 4.7 can be used to obtain the depletion widths corresponding to the p-GaAs emitter and n-GaAs base by

$$W_p = \frac{W}{\left(1 + \dfrac{N_{D_{emitter}}}{N_{D_{base}}}\right)},$$ (4.8)

$$W_n = \frac{W}{\left(1 + \dfrac{N_{D_{base}}}{N_{D_{emitter}}}\right)},$$ (4.9)

where N_D is the doping concentration of the specified region. The space charge regions identified by these calculations ensure an adequate number of mesh nodes are identified to provide the accurate calculation of carrier transport for this vital region. Figure 18 depicts close-up views of the mesh within the p-n junction of the virtual solar cell for both identified, Fig. 18a, and unidentified, Fig. 18b, space charge regions. In Fig. 18a, region 1 is the contact, regions 2 and 3 are vacuum, and region 4 is the AlGaAs window. The emitter is divided into two regions, region 5 is the neutral p-GaAs region of the emitter and region 6 is the space charge region of the emitter. Similarly, the base is divided into the base space charge region, region 7, and the neutral n-GaAs base region, region 8. The regions in Fig. 18b are similarly identified but without the emitter and base space charge regions. A comparison of the mesh layouts reveals a mesh with a significantly higher node density in the space charge region of the solar cell with an identified space charge region. In Fig. 18b, it can be seen that the area corresponding to the space charge region in the emitter, Fig. 18a (6), is completely omitted in the mesh layout and as a result, the vital region would be ignored during carrier generation and recombination calculations.

<div align="center">(a)   (b)</div>
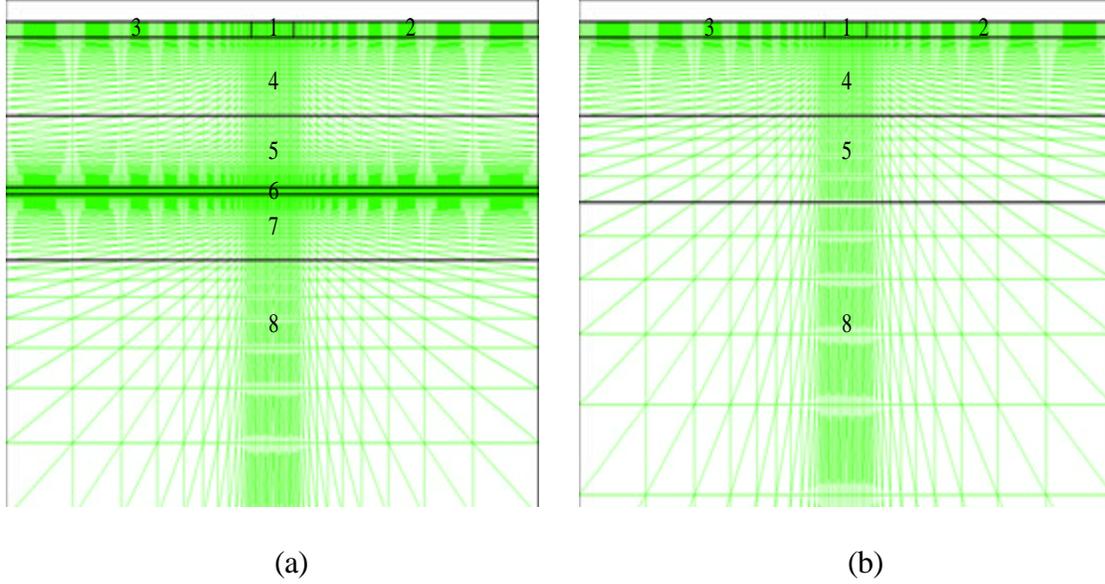
Figure 18.　　Mesh layout in the vicinity of the p-n junction in the virtual GaAs solar cell model with (a) specified and (b) unspecified space charge regions.

3.　　Material Models

ATLAS permits the user to identify a variety of models [Ref. 6] for calculating carrier mobility and recombination. The Concentration-Dependent Low Field Mobility model (CONMOB) was used to model the doping-dependent low-field mobilities of electrons and holes in GaAs at 300K. Through CONMOB, ATLAS provides empirical mobility data relative to doping concentrations specifically tailored for Si and GaAs [Ref. 6]. The recombination models utilized were the optical (OPTR) and the Shockley-Read-Hall (SRH) recombination models [Ref. 6]. The OPTR model was designed to be used with direct band gap materials such as GaAs. SRH recombination model takes into account the electrons being emitted or captured by donor and acceptor-like traps. ATLAS also provides a SRH Concentration-Dependent Lifetime (CONSRH) model where carrier lifetimes become a function of impurity concentrations [Ref. 6]. The application and limitations of these SRH models are discussed in the Analysis of Results Chapter of this thesis.

4.　　Trap Implementation

When implementing traps and defects ATLAS utilizes Poisson's equations in the form

$$\text{div}(e \nabla y) = q(n - p - N_D + N_A) + Q_T, \tag{4.10}$$

<div align="center">28</div>

where n and p are the carrier concentrations, N_D and N_A are the donor and acceptor con-centrations, and Q_T is total charge caused by the presence of traps. Q_T, is added to the right side of Poisson's equation [Ref. 6] with the value defined as

$$Q_T = q(p_t - n_t),\qquad(4.11)$$

where n_t and p_t are the densities of the trapped charge. These trapped charge densities are defined by,

$$n_t = N_t F_n,\qquad(4.12)$$

and

$$p_t = N_t F_p,\qquad(4.13)$$

where N_t is the density of traps, and F_n and F_p are the probabilities of occupation by carri-ers. The probabilities of occupation are based on the capture cross section and emission rates of the individually defined traps.

Based on Eqn. (4.10), ATLAS is capable of simulating a perfect crystal structure by setting Q_T equal to zero. However, this condition does not physically exist in large structures such as a solar cell. Impurities and defects associated with crystal growth are always present. To account for these defects, trap statements were implemented in the pre-irradiated solar cell model. Trap values prior to the application of radiation were not known for the referenced solar cells. Based on the LPE growth process, a trap energy level of 0.71 eV was selected for the pre-radiation model [Ref. 13]. The densities of these traps was interpreted based on the linear relationship between trap density and flu-ence level. The curve fit between data at fluence levels of 10^{14} and 10^{16} provides a linear relation ship in the form of

$$N_t = 0.027\Phi_e + 3\times10^{11},\qquad(4.14)$$

where N_t is the trap density and Φ_e is the electron fluence level. From Eqn. 4.14, the trap density for the pre-radiation model was determined to be of 3×10^{11} /cm^3. Traps in all other models were implemented in accordance with the referenced findings and previ-ously annotated interpolations.

Trap statements in ATLAS have a specific format and required information fields [Ref. 6]. A typical trap statement is expressed in the following form:

```
trap acceptor e.level=0.71 density=1e6 sign=4.0e13 sigp=4.0e15 region=5
```

The trap statement is initiated by the term `trap`. Traps are identified as acceptor- or donor-type traps. ATLAS defines acceptor traps as "hole traps" measured from the conduction band to the hole trap [Ref. 6]. Donor traps are defined as "electron traps" measured from the valence band to the electron trap, as shown in Fig. 19. This reveals that ATLAS utilizes holes in the conduction band and electrons in the valence band which is opposite to the definitions typically used by physicists [Ref. 11]. However, this program is meant to be integrated with complex electrical circuits and hole flow is in line with electrical engineering practices [Ref. 6]. As such, hole traps are implemented in the p-GaAs regions as acceptor traps while electron traps are implemented in the n-GaAs regions as donor traps.
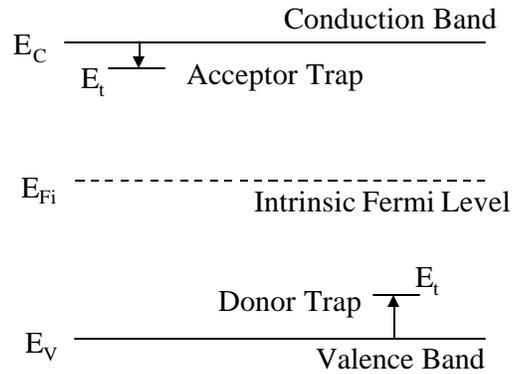
Figure 19.   Representation of Silvaco trap definitions [From Ref. 7.].

Capture cross sections are labeled as `sign` or `sigp` referring to the charge displayed by the trap. Prior to a trap capturing an electron or a hole, the capture cross section of a trap was implemented as that value measured experimentally for an oppositely-charged carrier [Ref. 6]. Once the trap has captured a carrier, it now becomes neutral and will have a smaller capture cross section [Ref. 6]. Measurements of neutral trap capture cross sections were not available in the referenced documentation. Each trap may be made up of a variety of situations. Some combinations may include a vacancy, an interstitial atom, multiple interstitials, multiple vacancies, or a combination of vacancies and

impurities [Ref. 14]. As a result, it is not known what exactly is causing a specific trap induced by radiation. It was speculated that the capture cross section of a neutral trap would be some constant ratio of the measured capture cross section value. This ratio was determined to be 1×10^{-2} through iterative simulations. To further elaborate, hole traps would display a greater capture cross section when negatively charged, represented in the value of the parameter `sign`, while having a smaller capture cross section when neutral represented in the parameter `sigp`. The proper implementation of traps was confusing to decipher with regards to the integrating of physics based data with an electrical engineering-based simulation. To clarify the implementation of traps, an example using characteristics one would encounter reading physics documentation and implementation of this data in ATLAS code, is provided.

A hole trap measured in the p-GaAs region with an energy level of E_t, a measured hole capture cross section of s_p, and a measured trap density of N_t would be implemented in the following manner:

```
trap acceptor e.level=Et density=Nt sign=sp sigp=(sp)*1e-2 region=
```

Similarly, an electron trap measured in the n-GaAs region with an energy level of E_t, a measured electron capture cross section of s_n, and a measured trap density of N_t would be implemented in the following manner:

```
trap donor e.level=Et density=Nt sign=(sn)*1e-2  sigp=sn region=
```

5.   Results of Simulation

The results of simulation are shown in Table 2 with reference to electron fluence levels, $?_e$. Short circuit currents and open circuit voltages were extracted from ATLAS output data. Maximum power, fill factor, and efficiency were calculated based on standard definitions. The virtual solar cell modeled with ATLAS demonstrates a 15% drop in open circuit voltage and 35% drop in short circuit current at the highest fluence levels. The model shows a 50% loss in efficiency and maximum power with a small degradation in fill factor.

Table 2.   Output characteristics of the virtual GaAs solar cell implemented in ATLAS.

	Pre-Rad	$\phi_e = 10^{14}$ e/cm^2	$\phi_e = 10^{15}$ e/cm^2	$\phi_e = 10^{16}$ e/cm^2
I_{SC}, mA	26.44	24.73	21.31	17.13
V_{OC}, V	0.996	0.969	0.889	0.843
P_{max}, mW	21.67	19.50	14.67	10.98
FF	0.823	0.814	0.775	0.766
Eff, %	16.48	14.83	11.16	8.35

The degradation in the *I-V* curve as a result of ele ctron radiation is shown in Fig. 20. The consistent shape of *I-V* curve was anticipated and is an indication of the fill factor's consistency over changes in fluence levels. The maximum power points are annotated with diamonds on their respective curves. These results are consistent with typical experimental results available in literature [Ref. 16].
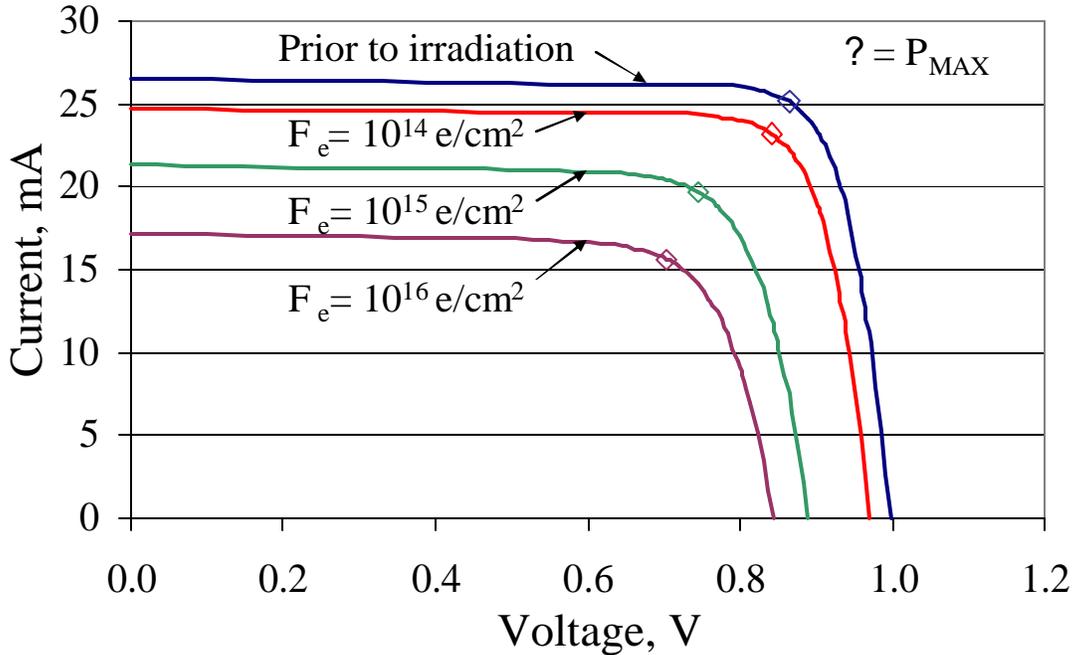
Figure 20.   Current-Voltage curve for the virtual GaAs solar cell as function of electron fluence level.

The spectral response curves of the virtual solar cell are shown in Fig. 21. The pre-irradiation curve shows a peak value of 81% at a wavelength of 0.65 µm. The deterioration of the spectral response is shown with reference to the associated fluence levels.
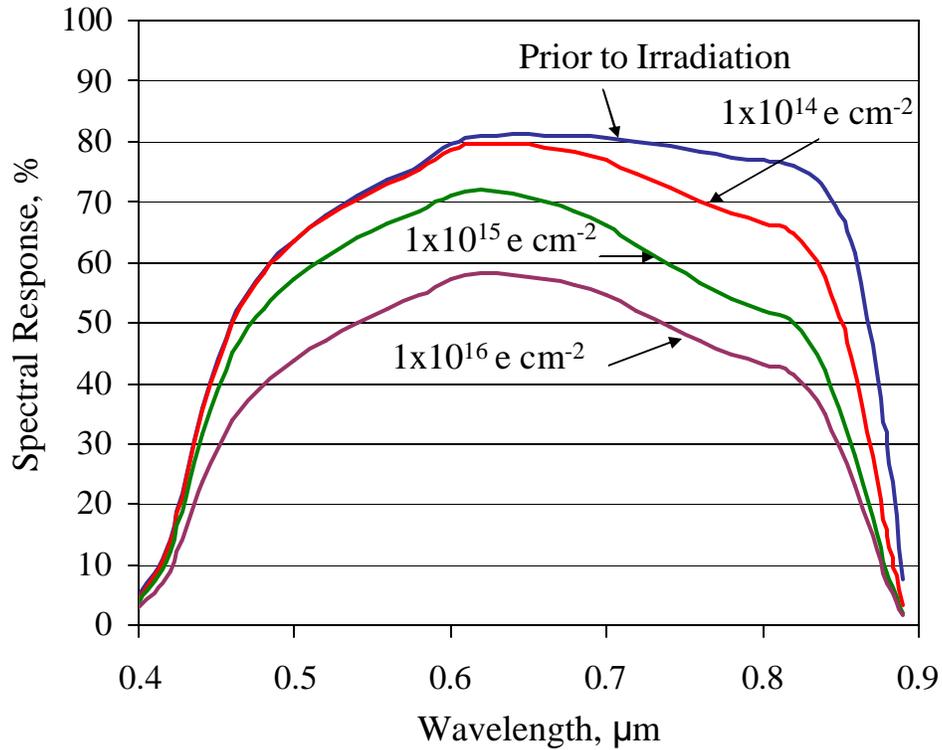
Figure 21.   Spectral response of the virtual solar cell with respect to radiation fluence levels.

Figure 22 shows a series of the virtual solar cell model structures overlaid with the photogeneration rates corresponding to the annotated wavelength. The EHP generations at shorter wavelengths occur uniformly across the cell. As the wavelength increases, the photogeneration increases deeper in to the solar cell. The shadow of the gold contact can be seen in the middle of the cell structure and it can be seen that gold at these small thicknesses permits the transmission of some light into the cell. The numbers listed in the are the Log_{10} of the photogeneration rates for the given wavelength.
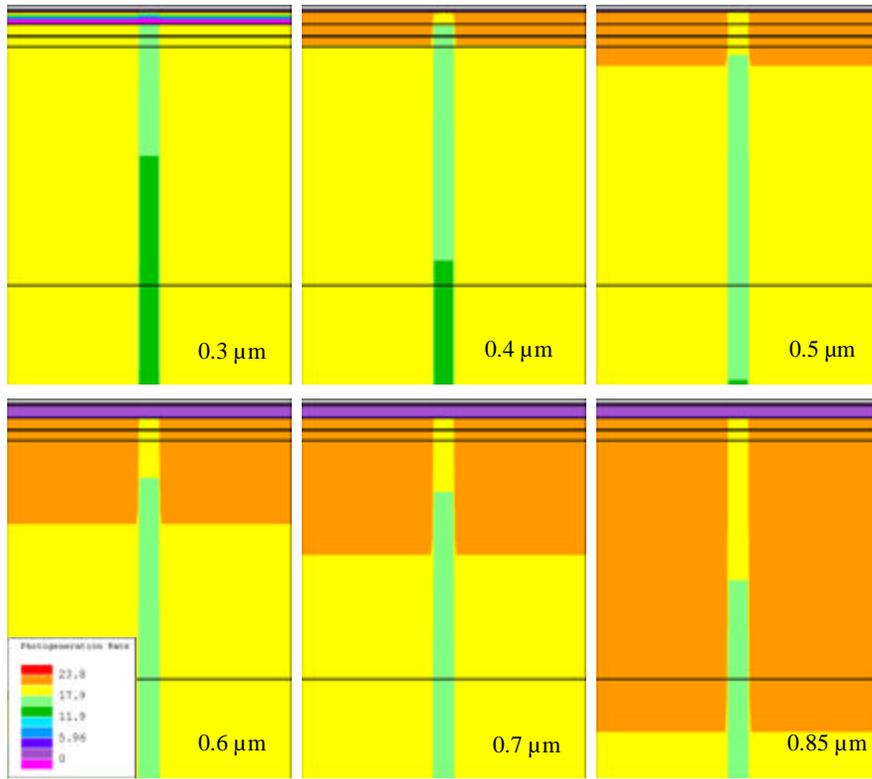
Figure 22.   Illumination of the virtual solar cell model and the resulting photogeneration rates with respect to various wavelengths.

The generation of photocurrent is only part of the output associated with an illuminated virtual solar cell model. Figure 23 shows the recombination rates associated with annotated wavelengths. At shorter wavelengths the highest recombination occurs in the AlGaAs window layer. As the wavelength increases, the recombination rate increases deeper into the solar cell. One can also notice that the space charge region has a consistently low recombination rate due to the inherent electrical field in this region.
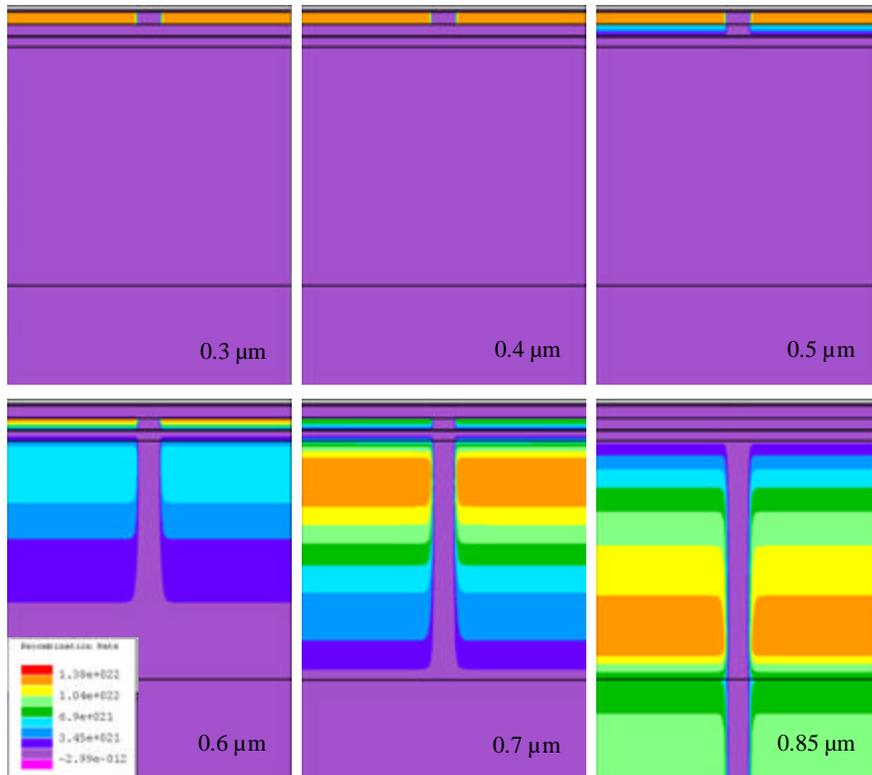
Figure 23.   Illumination of the virtual solar cell model and the resulting recombination
rates with respect to various wavelengths.

C.   SUMMARY

The parameters and techniques used to model the virtual solar cells in ATLAS
were presented and justified in this chapter. The output characteristics of the virtual solar
cells were shown to degrade with the implementation of traps associated with the three
levels of electron fluence. The following chapter compares these results to the measured
values of the referenced documentation and expounds upon possible causes of the more
significant deviations in values.

THIS PAGE INTENTIONALLY LEFT BLANK

V.   ANALYSIS OF RESULTS

In this chapter the results of the previous chapter are compared to the measured results presented in Chapter III. Some of the differences in output characteristics are discussed and potential causes are identified.

A.   DIRECT COMPARISON OF OUTPUT CHARACTERISTICS

The simulation results of the virtual solar cell model are tabulated and compared to the experimental values in Table 3. There is, on average, less than 3% error between measured and calculated parameters. Simulated and measured values of I_{SC}, V_{OC}, and fill factor are compared in Fig. 24 while maximum power and efficiency are compared in Fig. 25. In both graphs, the simulated data is represented by discrete points, while the measured data is represented by lines derived from several points selected from the originally published curves [Ref. 12]. The fill factor, as expected, is consistently high as a result of modeling with no resistance in the contacts.

Table 3.   Comparison of virtual model and experimentally measured output characteristics.

Parameter	Prior			1 Mev $Fe = 10^{14}$e/cm^2		
	Measured Values			Normalized Values		
	Meas. [Ref. 12]	Sim	Diff, %	Meas. [Ref. 12]	Sim	Diff, %
I_{SC}	-	26.44	-	0.94	0.936	0.48
V_{OC}	-	0.996	-	0.96	0.973	1.30
P_{max}, mW	21.25	21.67	2.0	20	19.50	2.53
FF	0.78	0.823	5.5	0.78	0.814	4.30
Eff, %	15.7	16.48	5.1	15.1	14.83	0.47

Parameter	1 Mev $Fe = 10^{15}$e/cm^2			1 Mev $Fe = 10^{16}$e/cm^2		
	Normalized Values			Normalized Values		
	Meas. [Ref. 12]	Sim	Diff, %	Meas. [Ref. 12]	Sim	Diff, %
I_{SC}	0.82	0.806	1.70	0.60	0.648	8.00
V_{OC}	0.91	0.892	2.00	0.84	0.846	0.77
P_{max}, mW	16	14.67	8.34	11.25	10.98	2.39
FF	0.77	0.775	0.58	0.76	0.766	0.81
Eff, %	11.8	11.16	5.52	8.3	8.35	0.61
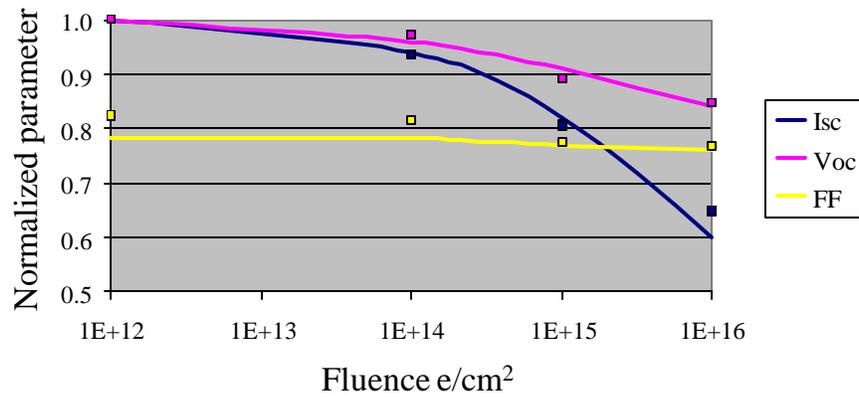
Figure 24.   Comparison of the virtual and experimentally measured solar cell's normalized I_{SC}, V_{OC}, and FF with respect to radiation fluence levels.
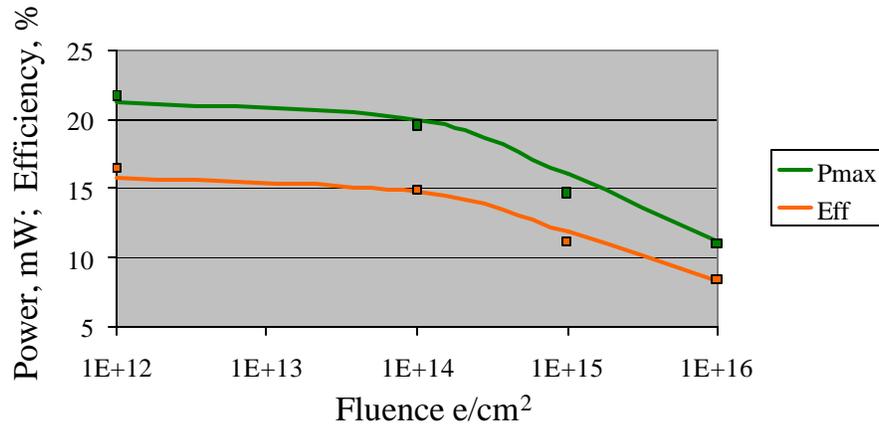
Figure 25.   Comparison of the virtual and experimentally measured solar cell's P_{max} and efficiency with respect to radiation fluence levels.

The results of the virtual solar cell for the fluence level of 10^{15} e/cm^2 demonstrate the greatest disagreement in maximum power. Both I_{SC} and V_{OC} are 2% below the measured values and the maximum power is 8% below the experimental measurement. This difference could be due to the inaccuracy of trap density information for this fluence level. As stated in Chapter II, the plot of trap densities showed a higher than expected value for the trap density at the hole trap with an energy of 0.71 eV. This energy level corresponds to a recombination center and would account for lower output characteristics at this fluence level. Reference sources provided no indication to the range of error in the measurements for trap densities.

At a fluence level of 10^{16} e/cm^2 there is an 8% difference in measured and simulated short circuit current. It is speculated that a programming limitation in the implementation of recombination models may be the source of this difference. GaAs has demonstrated trap induced carrier lifetime variations that are dependent upon doping concentrations [Ref. 17]. Shallow traps, near conduction and valence bands, demonstrate a reduction in carrier lifetime as the ratio of the doping concentration to the trap density is decreased. Deep level traps, near the intrinsic Fermi level, have been shown to be independent of doping concentrations. ATLAS has the ability to account for a concentration-dependent recombination model with the CONSRH model statement. However, recombination models are identified over specific regions and cannot be applied to individual trap statements within a region. Simulations with the CONSRH model produced a short circuit current value that was 9% below the measured output value at a fluence level of 10^{16} e/cm^2 while the SRH model was shown to produce a value 8% above the measured output value. A more accurate calculation may be obtainable if recombination models could be applied to specific trap statements.

B.   SPECTRAL RESPONSE

Figure 26 is a graphical representation of the experimentally measured spectral response of an actual GaAs solar cell with reference to electron fluence for wavelengths of light ranging from 0.4 µm to 0.9 µm. These values are normalized with respect to the maximum pre-radiation spectral response value. Similarly, the virtual solar cell's spectral response for the same radiation fluence levels are shown in Fig. 27. Both experimental and simulated spectral response curves show peak values around a wavelength of 0.65 µm. The peak values on both plots are approximately 98, 88 and 72 percent of the original response for fluence levels of 10^{14}, 10^{15} and 10^{16} e/cm^2, respectively. Significant deterioration in spectral response can be seen at the higher wavelengths where both curves show similar reductions in the longer wavelengths on the curves. Simulations in ATLAS produce an accurate representation of measured spectral response with respect to radiation fluence levels.
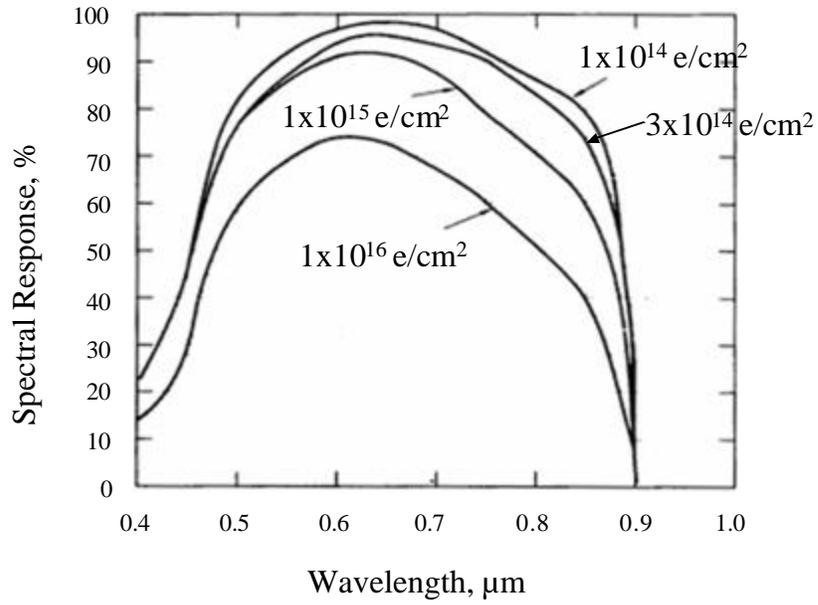
Figure 26.   Measured spectral response as a function of fluence [From Ref. 12.].
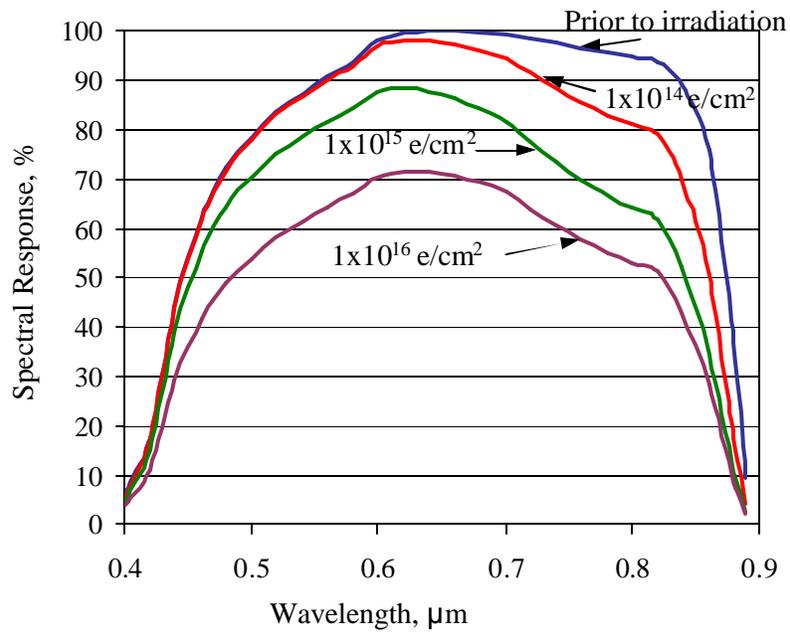
Figure 27.   Simulated spectral response as a function of fluence.

C.   SUMMARY

This chapter presented and compared several experimentally measured output characteristics with corresponding virtual solar cell model characteristics. A method to accurately predict the effects of radiation, based on the trap levels detected in the material after electron irradiation, was demonstrated. The following chapter presents the conclusions and recommendations for future study based on this work.

THIS PAGE INTENTIONALLY LEFT BLANK

VI. CONCLUSIONS AND RECOMMENDATIONS

The radiation modeling methodology demonstrated in this thesis utilizes measurable trap data to predict the degradation in output characteristics of solar cells. This differs from current methods of modeling and prediction which rely on extensive testing and data accumulation to develop empirical mathematical relationships between radiation fluence levels and solar cell output characteristics. The demonstrated method may reduce the testing required to characterize radiation damage in solar cells by capitalizing on the linear relationship between radiation fluence levels and trap density.

This thesis used published experimental information and measurements to virtually model the dimensions, materials and the effects of radiation on a p-on-n GaAs solar cell. The experimental measurements for this thesis were obtained from three primary publications. The first [Ref. 12] source provided the measurements for the output characteristics and the degrading effects of electron radiation. The remaining sources [Ref. 13 and 14] provided detailed trap characterization for grown-in and radiation induced defects in GaAs. Using this information a virtual solar cell model was created using Silvaco's ATLAS a physically based device simulator. Virtual GaAs solar cell models were created based on the documented dimensions, material and doping concentrations. The published trap information was used to model the effects of radiation in the virtual solar cells. Simulations with the virtual soar cell model illuminated with AM0 demonstrated an accurate representation of measured solar cell current, voltage, and spectral response values. The virtual solar cell demonstrated an accurate degradation in output characteristics when traps associated with corresponding fluence levels were implemented. The virtual solar cell model demonstrated accurate degradation over four fluence levels of electron radiation.

This method of modeling the effects of radiation can be used to predict the effects of radiation that produces uniform damage throughout the material [Ref. 19]. Electrons, neutrons, and high energy protons can be modeled using uniform trap implementation. Low energy proton radiation is a notable exception as it does not introduce damage uniformly within a semiconductor material [Ref. 12]. The penetration depth of low energy

protons is highly dependent upon energy levels resulting in a very complex trap density profile for which information was not immediately available.

This methodology may also prove useful in modeling the effects of annealing in solar cells. Annealing occurs when energy is added back to the crystal either through temperature or current injection. This energy allows for some displaced atoms to return to their proper placement in the crystal and thereby reducing the density of traps. Similar to radiation fluence, there is a linear relationship between the reduction in trap density and the time a solar cell is held at constant temperature [Ref. 12]. This relationship may prove useful in predicting solar cell annealing behavior with minimal testing requirements [Ref. 20].

This methodology shows the greatest potential with regards to multi-junction solar cells. ATLAS may provide the ability to predict the effects of radiation over the entire structure of a multi-junction cell based on information obtained from individual diodes of cells. The trap information required to model the effects of radiation can be obtained by irradiating separate p-n junctions produced of the same materials that make-up a multi-junction cell. The resulting trap information can be used to model the effects of radiation in the individual junctions and predict the degradation in the overall solar cell. Additionally, when used in conjunction with published optimization routines [Ref. 5], this methodology may be used to optimize multi-junction solar cells for power based on the projected end-of-life radiation exposure.

Physically based device simulation demonstrates promising potential to aid in the advancement of solar cell design [Ref. 20]. It can reduce the cost of design and production by minimizing testing requirements and optimizing structure design. This method of simulation may also provide a vehicle to exploit previously unused parameter relationship that may prove both accurate and insightful. Ultimately, the ability to reduce costs in design, testing and fabrication may aid in the proliferation of solar cells as a widely used renewable energy source. This work has been accepted for presentation at the 31st IEEE Photovoltaic Specialist Conference in Orlando, FL [Ref. 19 and 20].

APPENDIX A.   ATLAS INPUT DECKS

This appendix provides the ATLAS input decks used for this thesis. Section 1 provides the input deck for the pre-irradiation solar cell model. Section 2 provides the trap statements for the remaining fluence levels.

1.   PRE-IRRADIATION SOLAR CELL INPUT DECK

The following input deck was used to simulate the pre-irradiation GaAs solar cell model. The code provides for the calculation and plotting of the current-voltage characteristics curve, the dark current-voltage characteristics curve and extraction of data to plot the spectral response curve.

```
go atlas
mesh width=200000
#X-Mesh
x.mesh loc=-250 spac=62.5
x.mesh loc=-20 spac=2.5
x.mesh loc=20 spac=2.5
x.mesh loc=250 spac=62.5
#Y-Mesh
#Top contact
y.mesh loc=-211.1 spac=0.0125
y.mesh loc=-211 spac=0.0125
#Window
y.mesh loc=-211 spac=0.0625
y.mesh loc=-210.5 spac= 0.057293
# Emitter
y.mesh loc=-210.0417 spac=0.0052075
# Emitter Depletion Width
y.mesh loc=-210 spac=0.0052075
# Base Depletion Width
y.mesh loc=-209.5834 spac=0.052075
# Base
y.mesh loc=-205.2083 spac=1.1979
y.mesh loc=-200 spac=1.1979
# Substrate
y.mesh loc=0 spac=25
#Regions
# Contact
region num=1 material=Gold x.min=-20 x.max=20 y.min=-211.1 \
y.max=-211
region num=2 material=Vacuum x.min=-250 x.max=-20 y.min=-211.1 \
y.max=-211
region num=3 material=Vacuum x.min=20 x.max=250 y.min=-211.1 \
y.max=-211
# Window
region num=4 material=AlGaAs x.comp=0.95 x.min=-250 x.max=250 \
y.min=-211 y.max=-210.5
# Emmitter
```

```
region num=5 material=GaAs x.min=-250 x.max=250 y.min=-210.5 \
y.max=-210.0417
# Emmitter Depletion Region
region num=6 material=GaAs x.min=-250 x.max=250 y.min=-210.0417 \
y.max=-210
# Base Depletion Region
region num=7 material=GaAs x.min=-250 x.max=250 y.min=-210 \
y.max=-209.5834
# Base
region num=8 material=GaAs x.min=-250 x.max=250 y.min=-209.5834 \
y.max=-200
# Substrate
region num=9 material=GaAs x.min=-250 x.max=250 y.min=-200  \
y.max=0
#Electrodes
electrode name=anode material=Gold x.min=-20 x.max=20 \
y.min=-211.1 y.max=-211
electrode name=cathode material=Gold x.min=-250 x.max=250 \
y.min=0  y.max=0
#Doping
# Window
doping uniform region=4 p.type conc=1000000000000000000000
# Emitter
doping uniform region=5 p.type conc=1000000000000000000
# Emitter Depletion Region
doping uniform region=6 p.type conc=1000000000000000000
# Base Depletion Region
doping uniform region=7 n.type conc=100000000000000000
# Base
doping uniform region=8 n.type conc=100000000000000000
# Substrate
doping uniform region=9 n.type conc=500000000000000000
### Material properties ###
## Vacuum
material material=Vacuum real.index=3.3 imag.index=0
## GaAs (from
http://www.ioffe.rssi.ru/SVA/NSM/Semicond/GaAs/index.html)
material material=GaAs INDEX.FILE=opt/GaAsp.opt EG300=1.424
#PERMITTIVITY=12.9 AFFINITY=4.07 NC300=4.7e17 NV300=9e18 \
COPT=7.2e-10 NSRHN=5e18 NSRHP=5e18 TAUN0=5e-9 TAUP0=3e-6
## AlGaAs x=0.95
material material=AlGaAs INDEX.FILE=opt/AlGaAsx95.opt
#EG300=1.5487 PERMITTIVITY=12.616 AFFINITY=3.96 NC300=1.39e18 \
NV300=9.78e18 COPT=1.8e-10 TAUN0=4.5e-9 TAUP0=2e-8
## Gold
material material=Gold INDEX.FILE=opt/Gold.opt
############################################################
# Radiation effects                                       #
# Prior to Irradiation                                    #
############################################################
trap acceptor e.level=0.71 density=3.0e11 degen=2 sign=4e-013 \
sigp=4e-015 region=5
trap acceptor e.level=0.71 density=3.0e1 degen=2 sign=4e-013 \
sigp=4e-015 region=6
# Models
models region=4 ANALYTIC
models region=5 CONMOB BGN SRH
```

```
models region=6 CONMOB BGN SRH
models region=7 CONMOB SRH
models region=8 CONMOB SRH
models region=9 CONMOB SRH
models OPTR print
#Light beams
beam num=1 x.origin=0 y.origin=-710.5 angle=90 back.refl \
power.file=AM0nrel.spec wavel.start=0.12 wavel.end=0.75 \
wavel.num=630
beam num=2 x.origin=0 y.origin=-710.5 angle=90 back.refl \
power.file=AM0nrel.spec wavel.start=0.7501 wavel.end=2.4 \
wavel.num=825
##Structure File
struct outfile=structure/GaAs_LKL_0.str
log off
tonyplot structure/GaAs_LKL_0.str
############################################################
# Solves and plots light IV curve                         #
#                                                         #
############################################################
solve init
set I=0.95
method gummel newton maxtraps=10 itlimit=25
solve b1=0.9 b2=0.9
method newton maxtraps=10 itlimit=100
solve b1=$I b2=$I
extract name="isc" max(i."cathode")
set isc=$isc*200000
set i1=$isc/10
set i2=$i1+$isc/10
set i3=$i2+$isc/10
set i4=$i3+$isc/10
set i5=$i4+$isc/10
set i6=$i5+$isc/20
set i7=$i6+$isc/20
set i8=$i7+$isc/20
set i9=$i8+$isc/20
set i10=$i9+$isc/20
set i11=$i10+$isc/40
set i12=$i11+$isc/40
set i13=$i12+$isc/40
set i14=$i13+$isc/40
set i15=$i14+$isc/40
set i16=$i15+$isc/80
set i17=$i16+$isc/80
set i18=$i17+$isc/80
set i19=$i18+$isc/80
set i20=$i19+$isc/80
set i21=$i20+$isc/80
set i22=$i21+$isc/80
set i23=$i22+$isc/80
set i24=$i23+$isc/80
set i25=$i24+$isc/80
##Luminous Curve
contact name=anode current
method newton maxtraps=10 itlimit=100
log outfile=output/GaAs_LKL_0.log
```

```
solve ianode=-$i25 b1=$I b2=$I
solve ianode=-$i24 b1=$I b2=$I
solve ianode=-$i23 b1=$I b2=$I
solve ianode=-$i22 b1=$I b2=$I
solve ianode=-$i21 b1=$I b2=$I
solve ianode=-$i20 b1=$I b2=$I
solve ianode=-$i19 b1=$I b2=$I
solve ianode=-$i18 b1=$I b2=$I
solve ianode=-$i17 b1=$I b2=$I
solve ianode=-$i16 b1=$I b2=$I
solve ianode=-$i15 b1=$I b2=$I
solve ianode=-$i14 b1=$I b2=$I
solve ianode=-$i13 b1=$I b2=$I
solve ianode=-$i12 b1=$I b2=$I
solve ianode=-$i11 b1=$I b2=$I
solve ianode=-$i10 b1=$I b2=$I
solve ianode=-$i9 b1=$I b2=$I
solve ianode=-$i8 b1=$I b2=$I
solve ianode=-$i7 b1=$I b2=$I
solve ianode=-$i6 b1=$I b2=$I
solve ianode=-$i5 b1=$I b2=$I
solve ianode=-$i4 b1=$I b2=$I
solve ianode=-$i3 b1=$I b2=$I
solve ianode=-$i2 b1=$I b2=$I
solve ianode=-$i1 b1=$I b2=$I
solve ianode=0 b1=$I b2=$I
log off
tonyplot output/GaAs_LKL_0.log -set ivcurve.set
#############################################################
# Solves and plots the dark IV curve                       #
#                                                          #
#############################################################
solve init
method newton maxtraps=10 itlimit=100 CLIM.DD=1e8
contact name=anode
set Idrk=0
log outfile=output/drkGaAs_LKL_0.log
solve vanode=0.00 b1=$Idrk b2=$Idrk
solve vanode=0.20 b1=$Idrk b2=$Idrk
solve vanode=0.40 b1=$Idrk b2=$Idrk
solve vanode=0.60 b1=$Idrk b2=$Idrk
solve vanode=0.80 b1=$Idrk b2=$Idrk
solve vanode=0.82 b1=$Idrk b2=$Idrk
solve vanode=0.84 b1=$Idrk b2=$Idrk
solve vanode=0.86 b1=$Idrk b2=$Idrk
solve vanode=0.88 b1=$Idrk b2=$Idrk
solve vanode=0.90 b1=$Idrk b2=$Idrk
solve vanode=0.91 b1=$Idrk b2=$Idrk
solve vanode=0.92 b1=$Idrk b2=$Idrk
solve vanode=0.93 b1=$Idrk b2=$Idrk
solve vanode=0.94 b1=$Idrk b2=$Idrk
solve vanode=0.95 b1=$Idrk b2=$Idrk
solve vanode=0.96 b1=$Idrk b2=$Idrk
solve vanode=0.97 b1=$Idrk b2=$Idrk
solve vanode=0.98 b1=$Idrk b2=$Idrk
solve vanode=0.99 b1=$Idrk b2=$Idrk
solve vanode=1.00 b1=$Idrk b2=$Idrk
```

```
solve vanode=1.01 b1=$Idrk b2=$Idrk
solve vanode=1.02 b1=$Idrk b2=$Idrk
solve vanode=1.04 b1=$Idrk b2=$Idrk
solve vanode=1.06 b1=$Idrk b2=$Idrk
solve vanode=1.08 b1=$Idrk b2=$Idrk
solve vanode=1.10 b1=$Idrk b2=$Idrk
solve vanode=1.13 b1=$Idrk b2=$Idrk
solve vanode=1.16 b1=$Idrk b2=$Idrk
solve vanode=1.19 b1=$Idrk b2=$Idrk
solve vanode=1.22 b1=$Idrk b2=$Idrk
solve vanode=1.26 b1=$Idrk b2=$Idrk
solve vanode=1.32 b1=$Idrk b2=$Idrk
solve vanode=1.40 b1=$Idrk b2=$Idrk
log off
tonyplot output/drkGaAs_LKL_0.log
###############################################################
# Frequency log provides output for spectral response curve #
# Structure files provide pictures of photogeneration and    #
# recombination of carriers within the structure.            #
###############################################################
set I1=1.0
output con.band val.band
solve init
log outfile= output/GaAs_LKL_0_freq.log
contact name=anode
struc outfile=structure/illum/LKL0-0.20.str
solve vanode=0 b1=$I1 b2=$I1 lambda=0.2
struc outfile=structure/illum/LKL0-0.22.str
solve vanode=0 b1=$I1 b2=$I1 lambda=0.22
struc outfile=structure/illum/LKL0-0.24.str
solve vanode=0 b1=$I1 b2=$I1 lambda=0.24
struc outfile=structure/illum/LKL0-0.26.str
solve vanode=0 b1=$I1 b2=$I1 lambda=0.26
struc outfile=structure/illum/LKL0-0.28.str
solve vanode=0 b1=$I1 b2=$I1 lambda=0.28
struc outfile=structure/illum/LKL0-0.30.str
solve vanode=0 b1=$I1 b2=$I1 lambda=0.3
struc outfile=structure/illum/LKL0-0.32.str
solve vanode=0 b1=$I1 b2=$I1 lambda=0.32
struc outfile=structure/illum/LKL0-0.33.str
solve vanode=0 b1=$I1 b2=$I1 lambda=0.33
struc outfile=structure/illum/LKL0-0.335.str
solve vanode=0 b1=$I1 b2=$I1 lambda=0.335
struc outfile=structure/illum/LKL0-0.34.str
solve vanode=0 b1=$I1 b2=$I1 lambda=0.34
struc outfile=structure/illum/LKL0-0.35.str
solve vanode=0 b1=$I1 b2=$I1 lambda=0.35
struc outfile=structure/illum/LKL0-0.36.str
solve vanode=0 b1=$I1 b2=$I1 lambda=0.36
struc outfile=structure/illum/LKL0-0.38.str
solve vanode=0 b1=$I1 b2=$I1 lambda=0.38
struc outfile=structure/illum/LKL0-0.40.str
solve vanode=0 b1=$I1 b2=$I1 lambda=0.4
struc outfile=structure/illum/LKL0-0.42.str
solve vanode=0 b1=$I1 b2=$I1 lambda=0.42
struc outfile=structure/illum/LKL0-0.44.str
solve vanode=0 b1=$I1 b2=$I1 lambda=0.44
```

```
struc outfile=structure/illum/LKL0-0.46.str
solve vanode=0 b1=$I1 b2=$I1 lambda=0.46
struc outfile=structure/illum/LKL0-0.48.str
solve vanode=0 b1=$I1 b2=$I1 lambda=0.48
struc outfile=structure/illum/LKL0-0.50.str
solve vanode=0 b1=$I1 b2=$I1 lambda=0.5
struc outfile=structure/illum/LKL0-0.52.str
solve vanode=0 b1=$I1 b2=$I1 lambda=0.52
struc outfile=structure/illum/LKL0-0.54.str
solve vanode=0 b1=$I1 b2=$I1 lambda=0.54
struc outfile=structure/illum/LKL0-0.56.str
solve vanode=0 b1=$I1 b2=$I1 lambda=0.56
struc outfile=structure/illum/LKL0-0.58.str
solve vanode=0 b1=$I1 b2=$I1 lambda=0.58
struc outfile=structure/illum/LKL0-0.60.str
solve vanode=0 b1=$I1 b2=$I1 lambda=0.6
struc outfile=structure/illum/LKL0-0.62.str
solve vanode=0 b1=$I1 b2=$I1 lambda=0.62
struc outfile=structure/illum/LKL0-0.64.str
solve vanode=0 b1=$I1 b2=$I1 lambda=0.64
struc outfile=structure/illum/LKL0-0.66.str
solve vanode=0 b1=$I1 b2=$I1 lambda=0.66
struc outfile=structure/illum/LKL0-0.68.str
solve vanode=0 b1=$I1 b2=$I1 lambda=0.68
struc outfile=structure/illum/LKL0-0.70.str
solve vanode=0 b1=$I1 b2=$I1 lambda=0.7
struc outfile=structure/illum/LKL0-0.72.str
solve vanode=0 b1=$I1 b2=$I1 lambda=0.72
struc outfile=structure/illum/LKL0-0.74.str
solve vanode=0 b1=$I1 b2=$I1 lambda=0.74
struc outfile=structure/illum/LKL0-0.76.str
solve vanode=0 b1=$I1 b2=$I1 lambda=0.76
struc outfile=structure/illum/LKL0-0.78.str
solve vanode=0 b1=$I1 b2=$I1 lambda=0.78
struc outfile=structure/illum/LKL0-0.80.str
solve vanode=0 b1=$I1 b2=$I1 lambda=0.8
struc outfile=structure/illum/LKL0-0.82.str
solve vanode=0 b1=$I1 b2=$I1 lambda=0.82
struc outfile=structure/illum/LKL0-0.84.str
solve vanode=0 b1=$I1 b2=$I1 lambda=0.84
struc outfile=structure/illum/LKL0-0.86.str
solve vanode=0 b1=$I1 b2=$I1 lambda=0.86
struc outfile=structure/illum/LKL0-0.88.str
solve vanode=0 b1=$I1 b2=$I1 lambda=0.88
struc outfile=structure/illum/LKL0-0.89.str
solve vanode=0 b1=$I1 b2=$I1 lambda=0.89
struc outfile=structure/illum/LKL0-0.90.str
solve vanode=0 b1=$I1 b2=$I1 lambda=0.9
log off
```

2.   TRAP STATEMENTS FOR SIMULATED FLUENCE LEVELS

The following trap statements can be substituted within the input deck listed in Section 1. These traps represent the effects of 1 MeV electron radiation for fluence levels of 10^{14}e/cm^2, 10^{15}e/cm^2, 10^{16}e/cm^2.

```
##############################################################
# Radiation effects                                          #
# 1 MeV electron Fluence level 10to14 e/cm2                  #
##############################################################

trap acceptor e.level=0.71 density=3.0e12 degen=2 sign=4e-013 \
sigp=4e-015 region=5
trap acceptor e.level=0.71 density=3.0e12 degen=2 sign=4e-013 \
sigp=4e-015 region=6
trap donor e.level=0.14 density=1.8e13 degen=2 sigp=5.7e-013 \
sign=5.7e-015 region=7
trap donor e.level=0.41 density=8.2e13 degen=2 sigp=2.6e-013 \
sign=2.6e-015 region=7
trap donor e.level=0.71 density=3.0e10 degen=2 sigp=8.3e-013 \
sign=8.3e-015 region=7
trap donor e.level=0.90 density=8.8e11 degen=2 sigp=3e-011 \
sign=3e-013 region=7
trap donor e.level=0.14 density=1.8e13 degen=2 sigp=5.7e-013 \
sign=5.7e-015 region=8
trap donor e.level=0.41 density=8.2e13 degen=2 sigp=2.6e-013 \
sign=2.6e-015 region=8
trap donor e.level=0.71 density=3.0e10 degen=2 sigp=8.3e-013 \
sign=8.3e-015 region=8
trap donor e.level=0.90 density=8.8e11 degen=2 sigp=3e-011 \
sign=3e-013 region=8
trap donor e.level=0.14 density=1.8e13 degen=2 sigp=5.7e-013 \
sign=5.7e-015 region=9
trap donor e.level=0.41 density=8.2e13 degen=2 sigp=2.6e-013 \
sign=2.6e-015 region=9
trap donor e.level=0.71 density=3.0e10 degen=2 sigp=8.3e-013 \
sign=8.3e-015 region=9
trap donor e.level=0.90 density=8.8e11 degen=2 sigp=3e-011 \
sign=3e-013 region=9

##############################################################
# Radiation effects                                          #
# 1 MeV electron Fluence level 10to15 e/cm2                  #
##############################################################
trap acceptor e.level=0.13 density=2.2e14 degen=2 sign=2.6e-015 \
sigp=2.6e-017 region=5
trap acceptor e.level=0.29 density=4.0e14 degen=2 sign=2.6e-013 \
sigp=2.6e-015 region=5
trap acceptor e.level=0.35 density=8.0e13 degen=2 sign=6.4e-015 \
sigp=6.4e-017 region=5
trap acceptor e.level=0.71 density=6.4e13 degen=2 sign=4e-013 \
sigp=4e-015 region=5
trap acceptor e.level=0.13 density=2.2e14 degen=2 sign=2.6e-015 \
sigp=2.6e-017 region=6
trap acceptor e.level=0.29 density=4.0e14 degen=2 sign=2.6e-013 \
sigp=2.6e-015 region=6
trap acceptor e.level=0.35 density=8.0e13 degen=2 sign=6.4e-015 \
sigp=6.4e-017 region=6
trap acceptor e.level=0.71 density=6.4e13 degen=2 sign=4e-013 \
sigp=4e-015 region=6
trap donor e.level=0.41 density=2.1e13 degen=2 sigp=2.6e-013 \
sign=2.6e-015 region=7
```

```
trap donor e.level=0.71 density=1.7e13 degen=2 sigp=8.3e-013 \
sign=8.3e-015 region=7
trap donor e.level=0.90 density=2.8e13 degen=2 sigp=3e-011 \
sign=3e-013 region=7
trap donor e.level=0.41 density=2.1e13 degen=2 sigp=2.6e-013 \
sign=2.6e-015 region=8
trap donor e.level=0.71 density=1.7e13 degen=2 sigp=8.3e-013 \
sign=8.3e-015 region=8
trap donor e.level=0.90 density=2.8e13 degen=2 sigp=3e-011 \
sign=3e-013 region=8
trap donor e.level=0.41 density=2.1e13 degen=2 sigp=2.6e-013 \
sign=2.6e-015 region=9
trap donor e.level=0.71 density=1.7e13 degen=2 sigp=8.3e-013 \
sign=8.3e-015 region=9
trap donor e.level=0.90 density=2.8e13 degen=2 sigp=3e-011 \
sign=3e-013 region=9

#############################################################
# Radiation effects                                         #
# 1 MeV electron Fluence level 10to16 e/cm2                 #
#############################################################
trap acceptor e.level=0.13 density=8.4e14 degen=2 sign=2.6e-015 \
sigp=2.6e-017 region=5
trap acceptor e.level=0.29 density=1.6e15 degen=2 sign=2.6e-013 \
sigp=2.6e-015 region=5
trap acceptor e.level=0.35 density=1.0e15 degen=2 sign=6.4e-015 \
sigp=6.4e-017 region=5
trap acceptor e.level=0.71 density=2.7e14 degen=2 sign=4e-013 \
sigp=4e-015 region=5
trap acceptor e.level=0.13 density=8.4e14 degen=2 sign=2.6e-015 \
sigp=2.6e-017 region=6
trap acceptor e.level=0.29 density=1.6e15 degen=2 sign=2.6e-013 \
sigp=2.6e-015 region=6
trap acceptor e.level=0.35 density=1.0e15 degen=2 sign=6.4e-015 \
sigp=6.4e-017 region=6
trap acceptor e.level=0.71 density=2.7e14 degen=2 sign=4e-013 \
sigp=4e-015 region=6
trap donor e.level=0.41 density=8.8e13 degen=2 sigp=2.6e-013 \
sign=2.6e-015 region=7
trap donor e.level=0.71 density=5.0e13 degen=2 sigp=8.3e-013 \
sign=8.3e-015 region=7
trap donor e.level=0.90 density=6.5e13 degen=2 sigp=3e-011 \
sign=3e-013 region=7
trap donor e.level=0.41 density=8.8e13 degen=2 sigp=2.6e-013 \
sign=2.6e-015 region=8
trap donor e.level=0.71 density=5.0e13 degen=2 sigp=8.3e-013 \
sign=8.3e-015 region=8
trap donor e.level=0.90 density=6.5e13 degen=2 sigp=3e-011 \
sign=3e-013 region=8
trap donor e.level=0.41 density=8.8e13 degen=2 sigp=2.6e-013 \
sign=2.6e-015 region=9
trap donor e.level=0.71 density=5.0e13 degen=2 sigp=8.3e-013 \
sign=8.3e-015 region=9
trap donor e.level=0.90 density=6.5e13 degen=2 sigp=3e-011 \
sign=3e-013 region=9
```

APPENDIX B.   MATLAB SCRIPTS AND FUNCTIONS

MATLAB scripts and functions were used to produce input decks that could be modified and accurately reproduced during iterative solutions [Ref. 5]. During the research of this method of radiation modeling, it was import to have the capability to manipulate parameters that would now appear to be standardized. As such, these codes are not expressed in the most efficient method one would use model solar cells on a more broad scale. Section 1 is the MATLAB script to produce a comprehensive input deck specifying desired fluence levels and output requirements. Section 2 is a function that produces the bulk of the standard ATLAS input deck. Section 3 contains the functions to produce the lines of code that represent the various fluence levels.

1.   MATLAB CODE FOR PRIMARY INPUT FILE

The primary script file used to manipulate the desired output is *LKLcell1.m*. This file allows the designation of trap settings, fluence levels and output curves and data.

```
format long
fclose('all');
clear;
clc;
rdlvl='allsets'; % 0, 14, 15, 16 or 'allsets'
t='b';          % 'a' donors in the p region or 'b' acceptors in the p region
capt='cec';     % default 'chc' capture holes in p region or 'cec' capture electrons in the p-region
fac=1e-2;       % multiplication factor of capture cross section sigma
IVcurve=1;      % 1 produce IV output
drkcurve=1;     % 1 produce dark current output
specurve=1;     % 1 produce spectral response output
file=char(' ');
TRAPMOD='SRH';
if rdlvl=='allsets'
  for r=1:4
    rd=[0 14 15 16];
    radlvl=rd(r);
    if radlvl==0
      radpart=LKLrad0(t,capt,fac);
      file0=LKLSilv1(radlvl,radpart,t,capt,fac,IVcurve,drkcurve,specurve,TRAPMOD);
      file=char(file, file0);
      r=r+1;
    end
    if radlvl==14
      radpart=LKLrad14(t,capt,fac);
      file14=LKLSilv1(radlvl,radpart,t,capt,fac,IVcurve,drkcurve,specurve,TRAPMOD);
      file=char(file, file14);
      r=r+1;
    end
    if radlvl==15
      radpart=LKLrad15(t,capt,fac);
      file15=LKLSilv1(radlvl,radpart,t,capt,fac,IVcurve,drkcurve,specurve,TRAPMOD);
      file=char(file, file15);
      r=r+1;
    end
    if radlvl==16
      radpart=LKLrad16(t,capt,fac);
      file16=LKLSilv1(radlvl,radpart,t,capt,fac,IVcurve,drkcurve,specurve,TRAPMOD);
```

```
        file=char(file, file16);
      end
    end
  end
end

radlvl=rdlvl;
if radlvl==0
  radpart=LKLrad0(t,capt,fac);
  file=LKLSilv1(radlvl,radpart,t,capt,fac,IVcurve,drkcurve,specurve,TRAPMOD)
end
if radlvl==14
  radpart=LKLrad14(t,capt,fac);
  file=LKLSilv1(radlvl,radpart,t,capt,fac,IVcurve,drkcurve,specurve,TRAPMOD)
end
if radlvl==15
  radpart=LKLrad15(t,capt,fac);
  file=LKLSilv1(radlvl,radpart,t,capt,fac,IVcurve,drkcurve,specurve,TRAPMOD)
end
if radlvl==16
  radpart=LKLrad16(t,capt,fac);
  file=LKLSilv1(radlvl,radpart,t,capt,fac,IVcurve,drkcurve,specurve,TRAPMOD)
end

% overwrite previous input deck
infile=char(['LKL_All']);
f=fopen([infile '.in'],'w');

[x,y]=size(file);
for i=1:x
  fprintf(f,'%s\n',deblank(file(i,:)));
end

fclose(f);
```

2.   MATLAB CODE TO PRODUCE THE BULK SILVACO CODE

The bulk of the ATLAS code does not change with fluence levels. The solar cell

structure, material parameters, and calculative methods are kept standardized across solar

cell models. The *LKLSilv1.m* function produces this portion of the input deck.

```
function file=LKLSilv1(radlvl,radpart,t,capt,fac,IVcurve,drkcurve,specurve, TRAPMOD)
%PARAMETERS
fclose('all');
% GaAs Constants (external to Silvaco)
% emmissivity (F/m)
epsR=12.9;
epso=8.8542e-17;
% intrinsic
ni=1.79e6;
%Temperature
T=300;
e=1.60218e-19;
k=1.3806e-23;

%%Cell structure
%Cell Width (um)
cellW=500;

%Cap/Contact (%) optimum 8%
contWper=8;

%Contact
contTH=0.1;
```

```
%Window
windowTH=0.5;
winDop=1e18;

%Emmiter
EmTH=0.5;
Edop=1e18;

%Base
BaseTH=10;
Bdop=1e17;

%Substrate
subTH=200;
subDop=5e17;

% Depletion Layer

Vo=k*T*log(Bdop*Edop/((ni)^2))/e;
WDep=((2*epsR*epso*Vo*(Bdop+Edop))/(e*Bdop*Edop))^.5*10^6;
BDepTH=WDep/(1+Bdop/Edop);
EDepTH=WDep/(1+Edop/Bdop);

%Standard number of Divisions
divs=8;

% Cell Structure calculations  ###
%\Cell is built in two mirrored halves +/- fo zero axis  ie. ( ++@@^^ | ^^@@++ )

cellWDiv=cellW/divs;
width3d=100e6/cellW;
cellWHalf=cellW/2;
contW=0.01*contWper*cellWHalf;
contWDiv=contW/divs;

subLo=0;
subHi=subLo-subTH;
subDiv=subTH/divs;

BLo=subHi;
BHi=BLo-BaseTH+BDepTH;
BDiv=(BaseTH-BDepTH)/divs;

BMid=BLo-(BaseTH+BDepTH)/2;

BDepLo=BHi;
BDepHi=BDepLo-BDepTH;
BDepDiv=BDepTH/divs;

EmDepLo=BDepHi;
EmDepHi=EmDepLo-EDepTH;
EmDepDiv=EDepTH/divs;

EmLo=EmDepHi;
EmHi=EmLo-EmTH+EDepTH;
EmDiv=(EmTH-EDepTH)/divs;

windowLo=EmHi;
windowHi=windowLo-windowTH;
windowDiv=windowTH/divs;

contLo=windowHi;
contHi=contLo-contTH;
contDiv=contTH/divs;

lightY=EmHi-500;

file=char('go atlas',...
    ['mesh width=' num2str(width3d)], ...
    ['#X-Mesh'], ...
    ['x.mesh loc=-' num2str(cellWHalf) ' spac=' num2str(cellWDiv)], ...
```

```
    ['x.mesh loc=-' num2str(contW) ' spac=' num2str(contWDiv)], ...
    ['x.mesh loc=' num2str(contW) ' spac=' num2str(contWDiv)], ...
    ['x.mesh loc=' num2str(cellWHalf) ' spac=' num2str(cellWDiv)], ...
    ['#Y-Mesh'], ...
    ['#Top contact'], ...
    ['y.mesh loc=' num2str(contHi) ' spac=' num2str(contDiv)], ...
    ['y.mesh loc=' num2str(contLo) ' spac=' num2str(contDiv)], ...
    ['#Window'], ...
    ['y.mesh loc=' num2str(windowHi) ' spac=' num2str(windowDiv)], ...
    ['y.mesh loc=' num2str(windowLo) ' spac= ' num2str(EmDiv)], ...
    ['# Emitter'], ...
    ['y.mesh loc=' num2str(EmLo) ' spac=' num2str(EmDepDiv)], ...
    ['# Emitter Depletion Width'], ...
    ['y.mesh loc=' num2str(EmDepLo) ' spac=' num2str(EmDepDiv)], ...
    ['# Base Depletion Width'], ...
    ['y.mesh loc=' num2str(BDepLo) ' spac=' num2str(BDepDiv)], ...
    ['# Base'], ...
    ['y.mesh loc=' num2str(BMid) ' spac=' num2str(BDiv)], ...
    ['y.mesh loc=' num2str(BLo) ' spac=' num2str(BDiv)], ...
    ['# Substrate'], ...
    ['y.mesh loc=' num2str(subLo) ' spac=' num2str(subDiv)], ...
    ['#Regions'], ...
    ['# Contact'], ...
    ['region num=1 material=Gold x.min=-' num2str(contW) ' x.max=' num2str(contW) '
y.min=' num2str(contHi)  ' y.max=' num2str(contLo)], ...
    ['region num=2 material=Vacuum x.min=-' num2str(cellWHalf) ' x.max=-' num2str(contW)
' y.min=' num2str(contHi) ' y.max=' num2str(contLo)], ...
    ['region num=3 material=Vacuum x.min=' num2str(contW) ' x.max=' num2str(cellWHalf) '
y.min=' num2str(contHi) ' y.max=' num2str(contLo)], ...
    ['# Window'], ...
    ['region num=4 material=AlGaAs x.comp=0.95 x.min=-' num2str(cellWHalf) ' x.max='
num2str(cellWHalf) ' y.min=' num2str(windowHi) ' y.max=' num2str(windowLo)], ...
    ['# Emmitter'], ...
    ['region num=5 material=GaAs x.min=-' num2str(cellWHalf) ' x.max=' num2str(cellWHalf)
' y.min=' num2str(EmHi) ' y.max=' num2str(EmLo)], ...
    ['# Emmitter Depletion Region'], ...
    ['region num=6 material=GaAs x.min=-' num2str(cellWHalf) ' x.max=' num2str(cellWHalf)
' y.min=' num2str(EmDepHi) ' y.max=' num2str(EmDepLo)], ...
    ['# Base Depletion Region'], ...
    ['region num=7 material=GaAs x.min=-' num2str(cellWHalf) ' x.max=' num2str(cellWHalf)
' y.min=' num2str(BDepHi) ' y.max=' num2str(BDepLo)], ...
    ['# Base'], ...
    ['region num=8 material=GaAs x.min=-' num2str(cellWHalf) ' x.max=' num2str(cellWHalf)
' y.min=' num2str(BHi) ' y.max=' num2str(BLo)], ...
    ['# Substrate'], ...
    ['region num=9 material=GaAs x.min=-' num2str(cellWHalf) ' x.max=' num2str(cellWHalf)
' y.min=' num2str(subHi) ' y.max=' num2str(subLo)], ...
    ['#Electrodes'], ...
    ['electrode name=anode material=Gold x.min=-' num2str(contW) ' x.max=' num2str(contW)
' y.min=' num2str(contHi) ' y.max=' num2str(contLo)], ...
    ['electrode name=cathode material=Gold x.min=-' num2str(cellWHalf) ' x.max='
num2str(cellWHalf) ' y.min=' num2str(subLo) ' y.max=' num2str(subLo)], ...
    ['#Doping'], ...
    ['# Window'], ...
    ['doping uniform region=4 p.type conc=' num2str(winDop)], ...
    ['# Emitter'], ...
    ['doping uniform region=5 p.type conc=' num2str(Edop)], ...
    ['# Emitter Depletion Region'], ...
    ['doping uniform region=6 p.type conc=' num2str(Edop)], ...
    ['# Base Depletion Region'], ...
    ['doping uniform region=7 n.type conc=' num2str(Bdop)], ...
    ['# Base'], ...
    ['doping uniform region=8 n.type conc=' num2str(Bdop)], ...
    ['# Substrate'], ...
    ['doping uniform region=9 n.type conc=' num2str(subDop)], ...
    ['## Material properties ##'], ...
    ['# Vacuum'], ...
    ['material material=Vacuum real.index=3.3 imag.index=0'], ...
    ['# GaAs (from http://www.ioffe.rssi.ru/SVA/NSM/Semicond/GaAs/index.html)'], ...
    ['material material=GaAs INDEX.FILE=opt/GaAsp.opt EG300=1.424 '], ...
    ['#PERMITTIVITY=12.9 AFFINITY=4.07 NC300=4.7e17 NV300=9e18 COPT=7.2e-10 \'], ...
```

```
        ['#NSRHN=5e18 NSRHP=5e18 TAUN0=5e-9 TAUP0=3e-6'], ...
        ['## AlGaAs x=0.95'], ...
        ['material material=AlGaAs INDEX.FILE=opt/AlGaAsx95.opt '], ...
        ['#EG300=1.5487 PERMITTIVITY=12.616 AFFINITY=3.96 NC300=1.39e18 \'], ...
        ['#NV300=9.78e18 COPT=1.8e-10 TAUN0=4.5e-9 TAUP0=2e-8 '], ...
        ['# Gold'], ...
        ['material material=Gold INDEX.FILE=opt/Gold.opt'], ...
        ['##Radiation effects'], ...
        [ radpart ], ...
        ['# Models'], ...
        ['models region=4 ANALYTIC' ], ...
        ['models region=5 CONMOB BGN ' TRAPMOD], ...
        ['models region=6 CONMOB BGN ' TRAPMOD], ...
        ['models region=7 CONMOB ' TRAPMOD], ...
        ['models region=8 CONMOB ' TRAPMOD], ...
        ['models region=9 CONMOB ' TRAPMOD], ...
        ['models OPTR print'], ...
        ['#Light beams'], ...
        ['beam num=1 x.origin=0 y.origin=' num2str(lightY) ' angle=90 back.refl
power.file=AM0nrel.spec wavel.start=0.12 wavel.end=0.75 wavel.num=630'],...
        ['beam num=2 x.origin=0 y.origin=' num2str(lightY) ' angle=90 back.refl
power.file=AM0nrel.spec wavel.start=0.7501 wavel.end=2.4 wavel.num=825'],...
        ['##Structure File'], ...
        ['struct outfile=structure/GaAs_LKL_' num2str(radlvl) '.str'], ...
        ['log off'], ...
        ['#tonyplot structure/GaAs_LKL_' num2str(radlvl) '.str']);

if IVcurve==1
    file=char(file,'solve init', ...
        'set I=0.95', ...
        'method gummel newton maxtraps=10 itlimit=25', ...
        'solve b1=0.9 b2=0.9', ...
        'method newton maxtraps=10 itlimit=100', ...
        'solve b1=$I b2=$I', ...
        'extract name="isc" max(i."cathode")', ...
        ['set isc=$isc*' num2str(width3d)], ...
        'set i1=$isc/10', ...
        'set i2=$i1+$isc/10', ...
        'set i3=$i2+$isc/10', ...
        'set i4=$i3+$isc/10', ...
        'set i5=$i4+$isc/10', ...
        'set i6=$i5+$isc/20', ...
        'set i7=$i6+$isc/20', ...
        'set i8=$i7+$isc/20', ...
        'set i9=$i8+$isc/20', ...
        'set i10=$i9+$isc/20', ...
        'set i11=$i10+$isc/40', ...
        'set i12=$i11+$isc/40', ...
        'set i13=$i12+$isc/40', ...
        'set i14=$i13+$isc/40', ...
        'set i15=$i14+$isc/40', ...
        'set i16=$i15+$isc/80', ...
        'set i17=$i16+$isc/80', ...
        'set i18=$i17+$isc/80', ...
        'set i19=$i18+$isc/80', ...
        'set i20=$i19+$isc/80', ...
        'set i21=$i20+$isc/80', ...
        'set i22=$i21+$isc/80', ...
        'set i23=$i22+$isc/80', ...
        'set i24=$i23+$isc/80', ...
        'set i25=$i24+$isc/80', ...
        '##Luminous Curve', ...
        'contact name=anode current', ...
        'method newton maxtraps=10 itlimit=100', ...
        ['log outfile=output/GaAs_LKL_' num2str(radlvl) '.log'], ...
        'solve ianode=-$i25 b1=$I b2=$I', ...
        'solve ianode=-$i24 b1=$I b2=$I', ...
        'solve ianode=-$i23 b1=$I b2=$I', ...
        'solve ianode=-$i22 b1=$I b2=$I', ...
        'solve ianode=-$i21 b1=$I b2=$I', ...
        'solve ianode=-$i20 b1=$I b2=$I', ...
```

```
            'solve ianode=-$i19 b1=$I b2=$I', ...
            'solve ianode=-$i18 b1=$I b2=$I', ...
            'solve ianode=-$i17 b1=$I b2=$I', ...
            'solve ianode=-$i16 b1=$I b2=$I', ...
            'solve ianode=-$i15 b1=$I b2=$I', ...
            'solve ianode=-$i14 b1=$I b2=$I', ...
            'solve ianode=-$i13 b1=$I b2=$I', ...
            'solve ianode=-$i12 b1=$I b2=$I', ...
            'solve ianode=-$i11 b1=$I b2=$I', ...
            'solve ianode=-$i10 b1=$I b2=$I', ...
            'solve ianode=-$i9 b1=$I b2=$I', ...
            'solve ianode=-$i8 b1=$I b2=$I', ...
            'solve ianode=-$i7 b1=$I b2=$I', ...
            'solve ianode=-$i6 b1=$I b2=$I', ...
            'solve ianode=-$i5 b1=$I b2=$I', ...
            'solve ianode=-$i4 b1=$I b2=$I', ...
            'solve ianode=-$i3 b1=$I b2=$I', ...
            'solve ianode=-$i2 b1=$I b2=$I', ...
            'solve ianode=-$i1 b1=$I b2=$I', ...
            'solve ianode=0 b1=$I b2=$I', ...
            'log off', ...
            ['#tonyplot output/GaAs_LKL_' num2str(radlvl) '.log -set ivcurve.set']);
    end

    if drkcurve==1
        drkplot=1
        file=char(file,'solve init', ...
            'method newton maxtraps=10 itlimit=100 CLIM.DD=1e8', ...
            '##Solving Dark Current', ...
            'contact name=anode', ...
            'set Idrk=0', ...
            ['log outfile=output/drkGaAs_LKL_' num2str(radlvl) '.log'], ...
            'solve vanode=0.00 b1=$Idrk b2=$Idrk', ...
            'solve vanode=0.20 b1=$Idrk b2=$Idrk', ...
            'solve vanode=0.40 b1=$Idrk b2=$Idrk', ...
            'solve vanode=0.60 b1=$Idrk b2=$Idrk', ...
            'solve vanode=0.80 b1=$Idrk b2=$Idrk', ...
            'solve vanode=0.82 b1=$Idrk b2=$Idrk', ...
            'solve vanode=0.84 b1=$Idrk b2=$Idrk', ...
            'solve vanode=0.86 b1=$Idrk b2=$Idrk', ...
            'solve vanode=0.88 b1=$Idrk b2=$Idrk', ...
            'solve vanode=0.90 b1=$Idrk b2=$Idrk', ...
            'solve vanode=0.91 b1=$Idrk b2=$Idrk', ...
            'solve vanode=0.92 b1=$Idrk b2=$Idrk', ...
            'solve vanode=0.93 b1=$Idrk b2=$Idrk', ...
            'solve vanode=0.94 b1=$Idrk b2=$Idrk', ...
            'solve vanode=0.95 b1=$Idrk b2=$Idrk', ...
            'solve vanode=0.96 b1=$Idrk b2=$Idrk', ...
            'solve vanode=0.97 b1=$Idrk b2=$Idrk', ...
            'solve vanode=0.98 b1=$Idrk b2=$Idrk', ...
            'solve vanode=0.99 b1=$Idrk b2=$Idrk', ...
            'solve vanode=1.00 b1=$Idrk b2=$Idrk', ...
            'solve vanode=1.01 b1=$Idrk b2=$Idrk', ...
            'solve vanode=1.02 b1=$Idrk b2=$Idrk', ...
            'solve vanode=1.04 b1=$Idrk b2=$Idrk', ...
            'solve vanode=1.06 b1=$Idrk b2=$Idrk', ...
            'solve vanode=1.08 b1=$Idrk b2=$Idrk', ...
            'solve vanode=1.10 b1=$Idrk b2=$Idrk', ...
            'solve vanode=1.13 b1=$Idrk b2=$Idrk', ...
            'solve vanode=1.16 b1=$Idrk b2=$Idrk', ...
            'solve vanode=1.19 b1=$Idrk b2=$Idrk', ...
            'solve vanode=1.22 b1=$Idrk b2=$Idrk', ...
            'solve vanode=1.26 b1=$Idrk b2=$Idrk', ...
            'solve vanode=1.32 b1=$Idrk b2=$Idrk', ...
            'solve vanode=1.40 b1=$Idrk b2=$Idrk', ...
            'log off', ...
            ['tonyplot output/drkGaAs_LKL_' num2str(radlvl) '.log']);
    end

    if specurve==1
        specplot=1
```

58

```
file=char(file,'set I1=1.0', ...
    'output con.band val.band', ...
    'solve init', ...
    ['log outfile= output/GaAs_LKL_' num2str(radlvl) '_freq.log'], ...
    'contact name=anode', ...
    ['struc outfile=structure/illum/LKL' num2str(radlvl) '-0.20.str'], ...
    'solve vanode=0 b1=$I1 b2=$I1 lambda=0.2', ...
    ['struc outfile=structure/illum/LKL' num2str(radlvl) '-0.22.str'], ...
    'solve vanode=0 b1=$I1 b2=$I1 lambda=0.22', ...
    ['struc outfile=structure/illum/LKL' num2str(radlvl) '-0.24.str'], ...
    'solve vanode=0 b1=$I1 b2=$I1 lambda=0.24', ...
    ['struc outfile=structure/illum/LKL' num2str(radlvl) '-0.26.str'], ...
    'solve vanode=0 b1=$I1 b2=$I1 lambda=0.26', ...
    ['struc outfile=structure/illum/LKL' num2str(radlvl) '-0.28.str'], ...
    'solve vanode=0 b1=$I1 b2=$I1 lambda=0.28', ...
    ['struc outfile=structure/illum/LKL' num2str(radlvl) '-0.30.str'], ...
    'solve vanode=0 b1=$I1 b2=$I1 lambda=0.3', ...
    ['struc outfile=structure/illum/LKL' num2str(radlvl) '-0.32.str'], ...
    'solve vanode=0 b1=$I1 b2=$I1 lambda=0.32', ...
    ['struc outfile=structure/illum/LKL' num2str(radlvl) '-0.33.str'], ...
    'solve vanode=0 b1=$I1 b2=$I1 lambda=0.33', ...
    ['struc outfile=structure/illum/LKL' num2str(radlvl) '-0.335.str'], ...
    'solve vanode=0 b1=$I1 b2=$I1 lambda=0.335', ...
    ['struc outfile=structure/illum/LKL' num2str(radlvl) '-0.34.str'], ...
    'solve vanode=0 b1=$I1 b2=$I1 lambda=0.34', ...
    ['struc outfile=structure/illum/LKL' num2str(radlvl) '-0.35.str'], ...
    'solve vanode=0 b1=$I1 b2=$I1 lambda=0.35', ...
    ['struc outfile=structure/illum/LKL' num2str(radlvl) '-0.36.str'], ...
    'solve vanode=0 b1=$I1 b2=$I1 lambda=0.36', ...
    ['struc outfile=structure/illum/LKL' num2str(radlvl) '-0.38.str'], ...
    'solve vanode=0 b1=$I1 b2=$I1 lambda=0.38', ...
    ['struc outfile=structure/illum/LKL' num2str(radlvl) '-0.40.str'], ...
    'solve vanode=0 b1=$I1 b2=$I1 lambda=0.4', ...
    ['struc outfile=structure/illum/LKL' num2str(radlvl) '-0.42.str'], ...
    'solve vanode=0 b1=$I1 b2=$I1 lambda=0.42', ...
    ['struc outfile=structure/illum/LKL' num2str(radlvl) '-0.44.str'], ...
    'solve vanode=0 b1=$I1 b2=$I1 lambda=0.44', ...
    ['struc outfile=structure/illum/LKL' num2str(radlvl) '-0.46.str'], ...
    'solve vanode=0 b1=$I1 b2=$I1 lambda=0.46', ...
    ['struc outfile=structure/illum/LKL' num2str(radlvl) '-0.48.str'], ...
    'solve vanode=0 b1=$I1 b2=$I1 lambda=0.48', ...
    ['struc outfile=structure/illum/LKL' num2str(radlvl) '-0.50.str'], ...
    'solve vanode=0 b1=$I1 b2=$I1 lambda=0.5', ...
    ['struc outfile=structure/illum/LKL' num2str(radlvl) '-0.52.str'], ...
    'solve vanode=0 b1=$I1 b2=$I1 lambda=0.52', ...
    ['struc outfile=structure/illum/LKL' num2str(radlvl) '-0.54.str'], ...
    'solve vanode=0 b1=$I1 b2=$I1 lambda=0.54', ...
    ['struc outfile=structure/illum/LKL' num2str(radlvl) '-0.56.str'], ...
    'solve vanode=0 b1=$I1 b2=$I1 lambda=0.56', ...
    ['struc outfile=structure/illum/LKL' num2str(radlvl) '-0.58.str'], ...
    'solve vanode=0 b1=$I1 b2=$I1 lambda=0.58', ...
    ['struc outfile=structure/illum/LKL' num2str(radlvl) '-0.60.str'], ...
    'solve vanode=0 b1=$I1 b2=$I1 lambda=0.6', ...
    ['struc outfile=structure/illum/LKL' num2str(radlvl) '-0.62.str'], ...
    'solve vanode=0 b1=$I1 b2=$I1 lambda=0.62', ...
    ['struc outfile=structure/illum/LKL' num2str(radlvl) '-0.64.str'], ...
    'solve vanode=0 b1=$I1 b2=$I1 lambda=0.64', ...
    ['struc outfile=structure/illum/LKL' num2str(radlvl) '-0.66.str'], ...
    'solve vanode=0 b1=$I1 b2=$I1 lambda=0.66', ...
    ['struc outfile=structure/illum/LKL' num2str(radlvl) '-0.68.str'], ...
    'solve vanode=0 b1=$I1 b2=$I1 lambda=0.68', ...
    ['struc outfile=structure/illum/LKL' num2str(radlvl) '-0.70.str'], ...
    'solve vanode=0 b1=$I1 b2=$I1 lambda=0.7', ...
    ['struc outfile=structure/illum/LKL' num2str(radlvl) '-0.72.str'], ...
    'solve vanode=0 b1=$I1 b2=$I1 lambda=0.72', ...
    ['struc outfile=structure/illum/LKL' num2str(radlvl) '-0.74.str'], ...
    'solve vanode=0 b1=$I1 b2=$I1 lambda=0.74', ...
    ['struc outfile=structure/illum/LKL' num2str(radlvl) '-0.76.str'], ...
    'solve vanode=0 b1=$I1 b2=$I1 lambda=0.76', ...
    ['struc outfile=structure/illum/LKL' num2str(radlvl) '-0.78.str'], ...
    'solve vanode=0 b1=$I1 b2=$I1 lambda=0.78', ...
```

```
              ['struc outfile=structure/illum/LKL' num2str(radlvl) '-0.80.str'], ...
              'solve vanode=0 b1=$I1 b2=$I1 lambda=0.8', ...
              ['struc outfile=structure/illum/LKL' num2str(radlvl) '-0.82.str'], ...
              'solve vanode=0 b1=$I1 b2=$I1 lambda=0.82', ...
              ['struc outfile=structure/illum/LKL' num2str(radlvl) '-0.84.str'], ...
              'solve vanode=0 b1=$I1 b2=$I1 lambda=0.84', ...
              ['struc outfile=structure/illum/LKL' num2str(radlvl) '-0.86.str'], ...
              'solve vanode=0 b1=$I1 b2=$I1 lambda=0.86', ...
              ['struc outfile=structure/illum/LKL' num2str(radlvl) '-0.88.str'], ...
              'solve vanode=0 b1=$I1 b2=$I1 lambda=0.88', ...
              ['struc outfile=structure/illum/LKL' num2str(radlvl) '-0.89.str'], ...
              'solve vanode=0 b1=$I1 b2=$I1 lambda=0.89', ...
              ['struc outfile=structure/illum/LKL' num2str(radlvl) '-0.90.str'], ...
              'solve vanode=0 b1=$I1 b2=$I1 lambda=0.9', ...
              'log off');
end
```

3.   MATLAB CODE FOR RADIATION LEVELS

For each level of radiation fluence a different set of trap statements must be used
to represent the level of damage incurred. These functions are called by *LKLcel1l.m* ac-
cording to the specified fluence level.

a.   Function LKLrad0.m

The function *LKLrad0.m* produces the portion of the code that represents the
grown-in defects present in the pre-irradiated solar cell model.

```
function radpart=LKLrad0(t,capt,fac)

if t=='a';
    type1='acceptor';
    type2='donor';
elseif t=='b';
    type1='donor';
    type2='acceptor';
end

x='n';
y='p';

if capt=='cec'
    x='p';
    y='n';
end

sig13=5.7e-13;
sig41=2.6e-13;
siga71=8.3e-13;
sig90=3.0e-11;
sigb71=4.0e-13;

siga13=num2str(fac*sig13);
siga41=num2str(fac*sig41);
sigaa71=num2str(fac*siga71);
siga90=num2str(fac*sig90);
sigba71=num2str(fac*sigb71);

n=5;

radpart=char(['trap ' type2 ' e.level=0.71 density=3.0e11 degen=2 sig' y '='
num2str(sigb71) ' sig' x '=' sigba71 ' region=' num2str(n)]);

n=6;
```

60

```
radpart=char(radpart,['trap ' type2 ' e.level=0.71 density=3e11 degen=2 sig' y '='
num2str(sigb71) ' sig' x '=' sigba71 ' region=' num2str(n)]);
```

b.   **Function LKLrad14.m**

The function *LKLrad14.m* produces the portion of the code that represents the defects introduced by exposure to 1MeV electron radiation at a fluence level of 10^{14}e/cm^2.

```
function radpart=LKLrad14(t,capt,fac)

if t=='a';
    type1='acceptor';
    type2='donor';
elseif t=='b';
    type1='donor';
    type2='acceptor';
end

x='n';
y='p';

if capt=='cec'
    x='p';
    y='n';
end

sig13=5.7e-13;
sig41=2.6e-13;
siga71=8.3e-13;
sig90=3.0e-11;
sigb71=4.0e-13;

siga13=num2str(fac*sig13);
siga41=num2str(fac*sig41);
sigaa71=num2str(fac*siga71);
siga90=num2str(fac*sig90);
sigba71=num2str(fac*sigb71);

n=5;

radpart=char(['trap  ' type2 ' e.level=0.71  density=3.0e12  degen=2  sig' y '='
num2str(sigb71) ' sig' x '=' sigba71 ' region=' num2str(n)]);


n=6;

radpart=char(radpart,['trap  ' type2 ' e.level=0.71  density=3.0e12 degen=2 sig' y '='
num2str(sigb71) ' sig' x '=' sigba71 ' region=' num2str(n)]);


for n=7:9

radpart=char(radpart,['trap ' type1 ' e.level=0.14  density=1.8e13  degen=2 sig' x '='
num2str(sig13) ' sig' y '=' siga13 ' region=' num2str(n)], ...
['trap ' type1 ' e.level=0.41 density=8.2e13 degen=2 sig' x '=' num2str(sig41) ' sig' y
'=' siga41 ' region=' num2str(n)], ...
['trap ' type1 ' e.level=0.71 density=3.0e10 degen=2 sig' x '=' num2str(siga71) ' sig' y
'=' sigaa71 ' region=' num2str(n)], ...
['trap ' type1 ' e.level=0.90 density=8.8e11 degen=2 sig' x '=' num2str(sig90) ' sig' y
'=' siga90 ' region=' num2str(n)]);

end
```

c.   **Function LKLrad15.m**

The function *LKLrad15.m* produces the portion of the code that represents the defects introduced by exposure to 1MeV electron radiation at a fluence level of 10^{14}e/cm^2.

```
function radpart=LKLrad15(t,capt,fac)

if t=='a';
    type1='acceptor';
    type2='donor';
elseif t=='b';
    type1='donor';
    type2='acceptor';
end

x='n';
y='p';

if capt=='cec'
    x='p';
    y='n';
end

sig41=2.6e-13;
siga71=8.3e-13;
sig90=3.0e-11;
sig13=2.6e-15;
sig29=2.6e-13;
sig35=6.4e-15;
sigb71=4.0e-13;

siga41=num2str(fac*sig41);
sigaa71=num2str(fac*siga71);
siga90=num2str(fac*sig90);
siga13=num2str(fac*sig13);
siga29=num2str(fac*sig29);
siga35=num2str(fac*sig35);
sigba71=num2str(fac*sigb71);

n=5;

radpart=char(['trap ' type2 ' e.level=0.13 density=2.2e14 degen=2 sig' y '='
num2str(sig13) ' sig' x '=' siga13 ' region=' num2str(n)], ...
['trap ' type2 ' e.level=0.29 density=4.0e14 degen=2 sig' y '=' num2str(sig29) ' sig' x
'=' siga29 ' region=' num2str(n)], ...
['trap ' type2 ' e.level=0.35 density=8.0e13 degen=2 sig' y '=' num2str(sig35) ' sig' x
'=' siga35 ' region=' num2str(n)], ...
['trap ' type2 ' e.level=0.71 density=6.4e13 degen=2 sig' y '=' num2str(sigb71) ' sig' x
'=' sigba71 ' region=' num2str(n)]);

n=6;

radpart=char(radpart,['trap ' type2 ' e.level=0.13 density=2.2e14 degen=2 sig' y '='
num2str(sig13) ' sig' x '=' siga13 ' region=' num2str(n)], ...
['trap ' type2 ' e.level=0.29 density=4.0e14 degen=2 sig' y '=' num2str(sig29) ' sig' x
'=' siga29 ' region=' num2str(n)], ...
['trap ' type2 ' e.level=0.35 density=8.0e13 degen=2 sig' y '=' num2str(sig35) ' sig' x
'=' siga35 ' region=' num2str(n)], ...
['trap ' type2 ' e.level=0.71 density=6.4e13 degen=2 sig' y '=' num2str(sigb71) ' sig' x
'=' sigba71 ' region=' num2str(n)]);


for n=7:9

radpart=char(radpart,['trap ' type1 ' e.level=0.41 density=2.1e13 degen=2 sig' x '='
num2str(sig41) ' sig' y '=' siga41 ' region=' num2str(n)], ...
['trap ' type1 ' e.level=0.71 density=1.7e13 degen=2 sig' x '=' num2str(siga71) ' sig' y
'=' sigaa71 ' region=' num2str(n)], ...
['trap ' type1 ' e.level=0.90 density=2.8e13 degen=2 sig' x '=' num2str(sig90) ' sig' y
'=' siga90 ' region=' num2str(n)]);
```

```
end
```

d.   Function LKLrad16.m

The function *LKLrad16.m* produces the portion of the code that represents the defects introduced by exposure to 1MeV electron radiation at a fluence level of 10^{14}e/cm^2.

```
function radpart=LKLrad16(t,capt,fac)

if t=='a'
    type1='acceptor';
    type2='donor';
elseif t=='b'
    type1='donor';
    type2='acceptor';
end

x='n';
y='p';

if capt=='cec'
    x='p';
    y='n';
end

sig41=2.6e-13;
siga71=8.3e-13;
sig90=3.0e-11;
sig13=2.6e-15;
sig29=2.6e-13;
sig35=6.4e-15;
sigb71=4.0e-13;

siga41=num2str(fac*sig41);
sigaa71=num2str(fac*siga71);
siga90=num2str(fac*sig90);
siga13=num2str(fac*sig13);
siga29=num2str(fac*sig29);
siga35=num2str(fac*sig35);
sigba71=num2str(fac*sigb71);

n=5;

radpart=char(['trap ' type2 ' e.level=0.13 density=8.4e14 degen=2 sig' y '='
num2str(sig13) ' sig' x '=' siga13 ' region=' num2str(n)], ...
['trap ' type2 ' e.level=0.29 density=1.6e15 degen=2 sig' y '=' num2str(sig29) ' sig' x
'=' siga29 ' region=' num2str(n)], ...
['trap ' type2 ' e.level=0.35 density=1.0e15 degen=2 sig' y '=' num2str(sig35) ' sig' x
'=' siga35 ' region=' num2str(n)], ...
['trap ' type2 ' e.level=0.71 density=2.7e14 degen=2 sig' y '=' num2str(sigb71) ' sig' x
'=' sigba71 ' region=' num2str(n)]);

n=6;

radpart=char(radpart,['trap ' type2 ' e.level=0.13 density=8.4e14 degen=2 sig' y '='
num2str(sig13) ' sig' x '=' siga13 ' region=' num2str(n)], ...
['trap ' type2 ' e.level=0.29 density=1.6e15 degen=2 sig' y '=' num2str(sig29) ' sig' x
'=' siga29 ' region=' num2str(n)], ...
['trap ' type2 ' e.level=0.35 density=1.0e15 degen=2 sig' y '=' num2str(sig35) ' sig' x
'=' siga35 ' region=' num2str(n)], ...
['trap ' type2 ' e.level=0.71 density=2.7e14 degen=2 sig' y '=' num2str(sigb71) ' sig' x
'=' sigba71 ' region=' num2str(n)]);


for n=7:9

radpart=char(radpart,['trap ' type1 ' e.level=0.41 density=8.8e13 degen=2 sig' x '='
num2str(sig41) ' sig' y '=' siga41 ' region=' num2str(n)], ...
```

```
['trap ' type1 ' e.level=0.71 density=5.0e13 degen=2 sig' x '=' num2str(siga71) ' sig' y
'=' sigaa71 ' region=' num2str(n)], ...
['trap ' type1 ' e.level=0.90 density=6.5e13 degen=2 sig' x '=' num2str(sig90) ' sig' y
'=' siga90 ' region=' num2str(n)]);

end
```

LIST OF REFERENCES

1.   S. Michael, *EC3230 Lecture Notes*, Naval Postgraduate School, Winter 2004 (unpublished)

2.   National Aeronautics and Space Administration, *Solar Cell Array Design Handbook*, Jet Propulsion Laboratory, Pasadena, CA, Vol. 1, 1976.

3.   National Aeronautics and Space Administration, *Solar Cell Radiation Handbook*, Jet Propulsion Laboratory, Pasadena, CA,1989.

4.   M. Green, "The verification of Silvaco as a solar cell simulation tool and the design and optimization of a four-junction solar cell", Master's Thesis, Naval Postgraduate School, 2002.

5.   A. Bates, "Novel optimization techniques for multijunction solar cell design using Silvaco ATLAS", Master's Thesis, Naval Postgraduate School, 2003.

6.   *ATLAS User's Manual*, vols. 1-2, software version 5.6.0.R, Silvaco International, Sunnyvale, CA, 2003.

7.   Kasap, S.O., *Principles of Electronic Materials and Devices*, McGraw Hill, New York, 2002.

8.   Sze, S.M., *Physics of Semiconductor Devices*, John Wiley & Sons, Inc., New York, 1981.

9.   Hovel, H.J., *Semiconductors and Semimetals: Solar Cells*, Academic Press, New York, 1975.

10.   Roman, J. M., *State of the Art III-V Solar Cell Fabrication Technologies, Device Designs and Applications*, Advanced Photovoltaic Cell Design, University Autonoma de Madrid, Madrid, Spain.
http://www.uam.es/departamentos/ciencias/fisicamateriales/presentacionE.html, last accessed, Aug. 2004.

11.   Vavilov, V.S., *Effects of Radiation on Semiconductors*, Consultants Bureau, New York, 1965.

12.   Loo, R.Y., Kamath, G.S., and Li, S.S., "Radiation Damage and Annealing in GaAs Solar Cells", *IEEE Transactions on Electrical Devices*, Vol. 37, No. 2, pp. 485-497, Feb 1990.

13.   Li, S.S., and Loo, R.Y., "Deep-Level defects and numerical simulation of radiation damage in GaAs solar cells", *Solar Cells*, Iss. 31, pp. 349-377, 1991.

14.   Wang, W., *Study of Grown-in Defects and Radiation-Induced Defects in GaAs and Al$_x$Ga$_{1-x}$As,* PhD dissertation, University of Florida, 1984.

15.   Renewable Resource Data Center, National Renewable Energy Laboratory http://rredc.nrel.gov/solar/spectra/am0/NewAM0.xls, last accessed Sept 2004.

16.   National Aeronautics and Space Administration, Jet Propulsion Laboratory, *GaAs Solar Cell Handbook*, 1996.

17.   Ringel, S. A., and Rohatgi, A., "The Effects of Trap-Induced Lifetime Variations on the Design and Performance of High-Efficiency GaAs Solar Cells", *IEEE Transactions on Electrical Devices*, Vol. 38, No. 11, pp. 2402-2409, Nov 1991.

18.   Crespin, A. L. and Michael, S., "Modeling the Effects of Electron Radiation in Solar Cells", presented at the 22nd AIAA International Communications Satellite Systems Conference & Exhibit, Monterey, CA, May 9-12, 2004.

19.   Warner, J., Crespin, A., Walter, R., Michael, S., Messenger, S., and Summers, G., "Modeling the Proton Radiation Response of GaAs Solar Cells," accepted for publication and presentation at the 31st IEEE Photovoltaic Specialists Conference, Jan 3-7, 2005, Orlando, FL.

20.   Crespin, A. L. and Michael, S., "Modeling the Effects of 1Mev Electron Radiation in GaAs Solar Cells using Silvaco", accepted for publication and presentation at the 31st IEEE Photovoltaic Specialist Conference, January 3-7, 2005, Orlando, FL.

INITIAL DISTRIBUTION LIST

1. Defense Technical Information Center
   Ft. Belvoir, Virginia

2. Dudley Knox Library
   Naval Postgraduate School
   Monterey, California

3. Dr. John P. Powers, Chairman
   Department of Electrical and Computer Engineering
   Naval Postgraduate School
   Monterey, California

4. Dr. Sherif Michael
   Department of Electrical and Computer Engineering
   Naval Postgraduate School
   Monterey, California

5. Dr. Gamani Karunasiri
   Department of Physics
   Naval Postgraduate School
   Monterey, California

6. Marine Corps Representative
   Naval Postgraduate School
   Monterey, California

7. Director, Training and Education, MCCDC, Code C46
   Quantico, Virginia

8. Director, Marine Corps Research Center, MCCDC, Code C40RC
   Quantico, Virginia

9. Marine Corps Tactical Systems Support Activity (Attn: Operations Officer)
   Camp Pendleton, California

10. Major Aaron L. Crespin, USMC
    Denver, Colorado